POLITECNICO DI TORINO

Department of Mechanical and Aerospace Engineering

(DIMEAS)

Master's Degree in Biomedical Engineering

Design of a biomimetic electrospun scaffold for the in vitro modelling of cardiac fibrosis

Supervisor

Full Professor Valeria Chiono

Co-supervisors

Irene Carmagnola Ph.D.

Alice Zoso Ph.D.

Candidate

Mimma Maggio

Academic Year 2020/2021

Ai miei genitori e a mia sorella

Index

Abstract

Cardiovascular diseases (CVDs) are the leading cause of morbidity and mortality worldwide. Affecting millions of people, Myocardial Infarction (MI) and Heart Failure (HF) are the major causes of death among CVDs. MI provokes the massive cardiomyocyte (CMs) loss in the infarcted zone followed by a progressive remodeling of left ventricle. CMs death triggers an inflammatory response followed by the proliferation of cardiac fibroblasts (CFs) in the ischemic region and their differentiation into cardiac myofibroblasts (MyoFs). These events lead to the extracellular matrix (ECM) components overdeposition and tissue stiffening, impairing cardiac function and resulting in cardiac fibrosis. Due to the limited regenerative capacity of native CMs, cardiac tissue cannot self-renew and restore its normal function after an injury. Currently heart functionality can only be restored by heart transplantation, which has been limited by the shortage of organ donors and potential side-effects post transplantation, such as implant rejection and infection. A variety of new therapies are being tested to regenerate infarcted myocardium and many approaches have been explored to engineer cardiac fibrosis in vitro. In vitro models can resemble specific physiological functions and be used in early stage research to investigate the efficiency and safety of therapeutic agents. They allow to replicate tissue specific architecture, although they do not mimic the complexity of the whole organ.

The aim of this work was to design an in vitro model of human cardiac fibrotic tissue, able to mimic low thicknesses of early and late stage infarcted tissue, through bioartificial 2D scaffold with tailored topographical cues. Polycaprolactone (PCL) nanofibrous scaffolds were fabricated by electrospinning, with random and aligned morphology, mimicking the ECM architecture of early and late stage cardiac fibrotic tissue, respectively. Fibers had an average diameter of ~130 nm, uniform morphology and few defects.

Many researchers have analysed the native cardiac ECM protein composition, quantifying the changes in protein relative amounts before and after MI. These analyses revealed increased amounts of Collagen type I and Fibronectin (10-fold) content after MI. Thus, to better mimic the fibrotic cardiac ECM, PCL scaffolds were coated with Collagen type I/Fibronectin 70/30 wt/wt. The biomimetic coating was grafted on the scaffold surface by a two-step strategy: an adhesive pre-coating was deposited on the scaffold surface exploiting 3,4- Dihydroxy-D,L-phenylalanine (DOPA) polymerization (PCL-polyDOPA) and then Collagen type I and Fibronectin were grafted on the polyDOPA coating (PCL-polyDOPA/Collagen type

I/Fibronectin). The effectiveness of the biomimetic surface functionalization was assessed by several characterization analyses, such as Quartz Crystal Microbalance with Dissipation monitoring (QCM-D), immunofluorescence staining, colorimetric assay (BCA kit) and SEM. Coating stability to 7 days incubation in physiological media was assessed. Preliminary cellular tests using viability (Cell Titer Blue) and cytotoxicity assays (CytoTox-ONE) validated the effectiveness of the functionalized scaffolds in supporting hCFs adhesion, proliferation and activation.

Once completely validated, the proposed in vitro model will be used for preclinical drug screening and as a platform to reproduce cardiac fibrosis.

The work was part of BIORECAR ERC project (772168).

1.Introduction

1.1 Aim of the Work

The aim of this thesis work is the design of an *in vitro* model of human cardiac fibrotic tissue in order to obtain a platform to test regenerative strategies, that would replace/reduce *in vivo* experimentation according to 3Rs principle. *In vitro* models are powerful tools for the study of pathologies and for drugs/therapies screening, since they overcame both ethical issues and low predictivity associated with animals *in vivo* experimentation. This thesis work is part of Biorecar ERC-CoG 2017 project, which aims to develop a new cell direct reprogramming strategy to induce phenotype change from cardiac fibroblasts to cardiomyocytes, in order to regenerate post-infarct myocardial tissue. The proposed *in vitro* model consists of electrospun bioartificial PCL-based scaffold with random morphology, coated by a biomimetic protein coating based on human collagen type I and human fibronectin, on which Human Cardiac Fibroblasts (HCFs) are cultured. PCL-based scaffolds are fabricated by electrospinning in order to mimic the architecture of the pathological cardiac ECM. Random nanofibers are chosen as their morphology mimic the early stage of cardiac fibrosis. The scaffold must enable cell attachment, growth and proliferation and give proper topographical and biological stimuli to HCFs. In order to make the scaffold biomimetic and thus to promote cell adhesion, a protein biomimetic coating, based on collagen type I and fibronectin, was designed. The surface modification will involve two steps, the deposition of an adhesive polyDOPA pre-coating and the subsequent grafting of Collagen type I/Fibronectin. The design of the biomimetic coating was based on a detailed study of the composition of the extracellular matrix (ECM) of the pathological cardiac tissue, in order to properly mimic the pathological ECM and to sustain long-term HCFs cultures. The effectiveness of the surface functionalization will be assessed by several physic-chemical characterization (QCM-D, BCA kit, immunofluorescence staining). Finally, preliminary cell adhesion tests will be performed in order to validate the proposed cardiac fibrosis *in vitro* model.

1.2 Heart Failure

Heart failure (HF) is a growing epidemic worldwide, associated with significant morbidity, mortality and health care costs. Heart failure afflicts more than 10 million patients in the United States and western Europe alone, representing one of the most important health problems in these countries. In China, in 2000, the prevalence of chronic heart failure was 0.9% in a population aged between 35 and 74 years[1], [2]. Prognosis is poor for Heart failure; 30 day all-cause readmission rates of 19% have been reported in the USA. 1-year all-cause mortality for patients with acute heart failure was 17% and stable or ambulatory was 7%, and 12-month hospitalization rates were 44% for patients who were readmitted to hospital and 32% for patients receiving ambulatory care, in Europe. Similar data have been reported in the Asian Sudden Cardiac Death in Heart Failure registry, showing that 19,2% of patients died or were hospitalized for heart failure within 1 year. The Sub- Saharan Africa Survey of Heart Failure reported an estimated 6-month mortality of 17,8%. The International Congestive Heart Failure study representing Africa, China, India, the Middle East, southeast Asia, and South America, reported an overall 1-year mortality of 16,5%, with substantial variation by region (34% in Africa, 23% in India, 15% in southeast Asia, 9% in South America, 9% in the Middle East, and 7% in China [3]. Due to the high and increasing prevalence rates, HF constitutes an enormous economic burden for the healthcare systems in industrialized countries. For example, Europe and USA spent 1–2% of their annual healthcare budget on HF. The global economic burden of HF is estimated at $108 billons per annum, with $65 billons attributed to direct and $43 billons to indirect costs. The US is the biggest contributor to the global HF costs and is responsible for 28.4% of total global HF spend. Europe accounts for 6.83% of total global HF costs [4].

Patients with end stage heart failure have a dismal prognosis and poor quality of life. Heart transplantation (HT) is the gold standard treatment for end-stage HF and it provides an effective treatment for a subset of these patients. HT significantly increases survival, exercise capacity, quality of life and return to work compared with conventional treatment. Apart from the shortage of donor hearts, the main challenges in transplantation are the consequences of the limited effectiveness and complications of immunosuppressive therapy in the long term (i.e. antibody-mediated rejection, infection, hypertension, renal failure, malignancy and coronary artery vasculopathy). In 2018, 3408 heart transplantations were performed in the United States. For transplantations that occurred between 2008 and 2015, the 1-year survival rate was 90.5%

for males and 91.1% for females and the 5-year survival rates were 78.4% for males and 77.7% for females [5]. After HT, patients may develop graft dysfunction, leading to native heart failure (HF). Despite advances in immunosuppressive agents, acute rejection and chronic rejection remain the major causes of graft failure (GF) after heart transplantation (HT). Graft rejection involves immune responses and inflammation. In acute rejection, expression of adhesion molecules by graft endothelial cells is increased, and inflammatory cells, including T cells and macrophages, infiltrate into the allografts and produce various cytokines and chemokines. In chronic rejection, graft vasculopathy is characterized by intimal thickening resulting from infiltration of inflammatory cells, proliferation of smooth muscle cells (SMCs), and accumulation of extracellular matrix. Due to the imbalance between demand for organs and supply of organ donors and medical contraindications to heart transplantation mentioned above, mechanical circulatory support (MCS) such as left ventricular assist devices (LVAD) have shown to be very beneficial as a bridge to transplantation and a big therapeutic opening, which will save lives.

Heart failure is a chronic, progressive condition consisting in heart's pumping efficiency impairment and it is caused by a variety of diseases, including ischemic heart disease, hypertensive heart disease, valvular heart disease and primary myocardial disease [6]. Risk factor such as coronary heart disease (CHD), hypertension, diabetes mellitus (DM), obesity and smoking are responsible for 52% incident HF cases in the population.[5] Patients affected with HF experiences a series of symptoms worsening their quality of life, including dyspnea, fatigue and weakness, oedema in lower limbs and rapid or irregular heartbeat. Cardiac fibrosis after myocardial infarction (MI) plays a key role in regulating heart function in the development of heart failure. It can determine the size, shape and wall thickness of ventricles.

Many factors limited the development of antifibrotic therapies for patients affected by cardiovascular diseases (CVD). First, adult human heart has a weak endogenous regenerative potential since cardiomyocytes (CMs) terminally differentiated cells with a poor proliferative capacity. This restricts therapies that aim to inhibit fibrosis entirely as the native CMs are unable to replace lost muscle tissue, thus increasing risk of cardiac rupture. Second, the molecular mechanisms driving cardiac fibrosis are complex and not fully understood. Moreover, the injured heart, after myocardial infarction (MI), is an hostile microenvironment that may hinder the efficacy of delivering antifibrotic therapies [7]. The goals of treatment in patients with HF are to improve their clinical status, functional capacity and quality of life, prevent hospitalization and reduce mortality. Traditional treatments aim to suppress symptoms deriving

from excessive electrical and biochemical remodeling, latest therapies, instead, focus on redirecting the scarring mechanism into a regenerative one.

Current available pharmacological treatments of cardiac fibrosis aims to reduce the workload, using diuretics and nitrates, and to inhibit the effects of toxic humoral factors overexpressed in HF, using β-blockers, angiotensin-converting enzyme inhibitors (ACEIs), Angiotensin receptor neprilysin inhibitors (ARNIs) and mineralocorticoid/aldosterone receptor antagonists (MRAs). ACEIs and receptor blockers act on renin-angiotensin-aldosterone system (RAAS) thereby they can alleviate cardiac fibrosis by reducing cardiac myofibroblasts number. Another alternative is to use hormonal targeting: Angiotensin II type I receptor blockers (ARBs), such as candesartan and valsartan, are used to inhibit remodeling. An alternative to pharmacological treatment is the use of non-surgical devices, in particular the implantation of cardioverter-defibrillator (ICDS) or the implantation of a pacemaker for the cardiac resynchronization therapy (CRT). Unfortunately, both drugs and interventional therapies cannot control disease progression to the end stage [8].

1.3 Myocardial Infarction

Myocardial infarction is a major cause of death and disability worldwide, it causes the death of billions of cardiomyocytes in the infarcted zone followed by a progressive pathological remodeling of the left ventricle (LV). In fact, during a myocardial infarction, sudden cardiomyocytes death triggers an acute, but transient, inflammatory response, led by circulating bone marrow–derived blood cells (BMCs), which is followed by the mobilization of cardiac fibroblasts (CFs) in the ischemic region.

Repair of the infarcted myocardium can be described in three overlapping phases: the inflammatory phase, the proliferative phase and the maturation phase. Approximately 3 days after MI, the infarct area is infiltrated by macrophages and phenotypically modified fibroblasts (myofibroblasts) that form granulation tissue in which ECM-degrading proteases of the matrix metalloproteinase (MMP) family and pro-angiogenic molecules such as vascular endothelial growth factor (VEGF) are up-regulated. The proliferative stage of remodeling is characterized by the clearance of dead cells, the breakdown of ECM and stimulation of angiogenesis to revascularize the ischemic tissue. Matrix degradation can increase inflammation by producing matrix fragments, such as matrikines along with proteolytic activation of TNF-α. The transition from the inflammatory phase to the fibrotic stage of remodeling (“maturation”) typically occurs 3–7 days post-MI and appears to be mediated by increased production of anti-inflammatory and

profibrotic factors such as transforming growth factor-ß (TGFß) and IL-10, derived from both infiltrating immune cells and myocardial cells. In response to such factors, myofibroblasts synthesize increased amounts of structural ECM proteins, particularly type I and III fibrillar collagens, to facilitate scar formation. This response is essential to replace the dead cardiomyocytes and prevent the myocardial wall rupture. Balanced ECM remodeling is crucial, since inadequate strength of the myocardial wall will lead to cardiac dilation, while excessive or prolonged ECM accumulation can result in fibrosis. While cardiac dilation primarily affects systolic function, fibrosis stiffens the myocardium and mainly obstruct the diastolic filling phase. Apoptosis of the majority of reparative cells marks the end of the proliferative phase, as the infarct matures and a scar comprised of cross-linked collagen is formed leading, over time, to a condition of cardiac fibrosis, that impairs the mechano-electric coupling of cardiomyocytes. Although fibrosis of the scar is an important and necessary response to injury, fibrosis remote to the scar, in the viable non-infarcted myocardium, contributes adversely to tissue structure and function, causing myocardial stiffness, cardiac dysfunction, and, ultimately, heart failure [9]–[11].

1.4 Myocardium morphology and physiology

Myocardium is a highly organized structure that consists of several cell types, such as cardiomyocytes, fibroblasts, endothelial cells (ECs), macrophages, and vascular and neuronal networks. Interspersed between these elements, the interstitium comprises a complex extracellular matrix (ECM) of structural, adhesive and matricellular proteins and cell-surface receptors (integrins) within a hydrated proteoglycan and glycosaminoglycan-rich milieu. The collagen proteins present in the myocardium include types I,III, IV, V and VI. Among these collagen type I is the predominant component (>70%) [12]. Cardiomyocytes occupy from 70% to 85% of the volume of the mammalian heart and they are the cells responsible for generating contractile force in the intact heart and they undergo enlargement (hypertrophy) in response to chronic demand for increased contractile force leading to insufficient output for demands of the whole organism (heart failure). Although non-myocytes occupy a relatively small volume fraction, they are essential for normal heart homeostasis, providing the extracellular matrix, intercellular communication and vascular supply needed for efficient cardiomyocytes contraction and long-term survival [13], [14]. Cardiac myocytes make up the bulk of the myocardial volume, but the cardiac fibroblasts (CFs) are the most numerous cell type in the heart, accounting about two-third of the cells. Under normal physiological conditions, CFs are

relatively inert cells that maintain myocardial ECM homeostasis. However, in response to cardiac injury or stress, they can adopt a specialized myofibroblasts phenotype that enables the cell to respond more effectively to environmental stimuli. Many studies showed that CFs are involved in the synthesis and remodeling of heart ECM and they are intricately involved in myocardial development and pathologies characterized by changes in the ECM, including hypertension and myocardial infarction [9], [15].

The ECM is the acellular components of the heart, it includes interstitial collagens, proteoglycans, glycoproteins, cytokines, growth factors, matrikines, and proteases. The extracellular matrix serves multiple purposes, because it forms an organizational network that surrounds and interconnects cells and provides a scaffold for cardiac cell populations. In addition, the ECM helps to distribute mechanical forces throughout the myocardium, convey mechanical signals to individual cells via cell surface ECM receptors, and participate in fluid movement in the extracellular environment [16]. The ECM components are also of key importance for preserving myocardial function under pathological conditions. A number of ECM proteins bind growth factors released during myocardial damage. Moreover, the products of ECM degradation subsequent to myocardial damage bind receptors for various growth factors and activate many signaling pathways. The interaction between the ECM and cells represents the essential moderator of adaptive and reparative changes of the myocardium as a reaction to various types of damage. This is enabled by a change in the cell phenotype as well as changes in the number, proportion and composition of ECM proteins [17].

1.4.1 Cardiac Fibroblasts

Cardiac fibroblasts (CFs) are the most abundant cell type in the mammalian heart and comprise approximately two-thirds of the total number of cardiac cell types. At the cellular level, the normal adult human heart comprises 30% cardiomyocytes and 70% non-myocytes, of which the majority are CFs. Cardiac Fibroblasts are mesenchymal cells, morphologically spindle-shaped and they are unique among other cell types since they lack a basement membrane. CFs are arranged in sheets and strands that run in parallel with muscle fibers and maintain continuity between cells in the different layers of the myocardium.[18] In the heart, myocytes are arranged in laminae that are organized into layers of myocytes approximately two to five cells thick. These layers of myocytes are surrounded by an endomysial collagen network, where cardiac fibroblasts interconnect with myocytes, and endothelial cells and vascular smooth muscle cells

are largely confined to the coronary vasculature. This arrangement of fibroblasts in vivo allows the fibroblasts to contract the endomysial collagen, exerting force on the myocytes. Importantly, the intercellular connections of fibroblasts appear to be via at least two different types of cell-cell molecules: connexins and cadherins [15]. CFs are involved in many aspects of cardiac functions, such as homeostasis and remodeling of the cardiac ECM, cell–cell communication with cardiomyocytes, electrical activity, production of growth factors and cytokines, and intercellular signaling with other CFs, endothelial or smooth muscle cells that can impact cellular events such as angiogenesis, cell proliferation, cardiomyocyte hypertrophy or apoptosis (Figure 1). CFs are connected with CMs via gap junctions, particularly connexin 45, which is essential in maintaining an optimal electrical conduction in the heart, while they form intercellular gap junctions through connexin 40. Another major function of CF is to synthesize a variety of bioactive molecules and secrete them into the myocardial interstitium. These molecules include cytokines (TNFα, interleukins and TGFβ), active peptides (angiotensin II, endothelin 1) and growth factors, which function in the myocardium in autocrine and/or paracrine fashions. CFs are the key cell type responsible for ECM homeostasis in health and its remodeling in heart disease. They synthesize the ECM proteins while also producing the enzymes that degrade these proteins, and inhibitors of these enzymes [19]. CFs are involved in the mechanism of cardiac fibrosis, in response to fibrotic stimuli, they differentiate into an activated state, myofibroblasts (MyoFs), secreting higher quantities of matrix proteins and exhibiting higher migration and contractility.

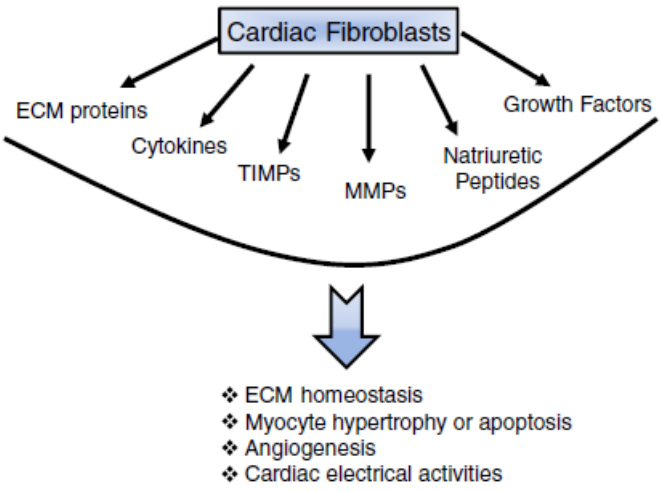

Figure 1. Cardiac fibroblasts impact different aspects of cardiac structure and function.

1.4.2 Bioactivity and Homeostasis of the Extracellular Matrix

The ECM is a highly dynamic noncellular 3-dimensional network that is present in all tissues and plays a critical role in homeostasis and disease. The ECM not only preserves structural and mechanical integrity, but also works as a signaling hub that transduces critical cascades for cell function, and as a reservoir of growth factors that can be released following injury to modulate cell behavior and to activate a reparative program [20]. An appropriate balance of extracellular matrix synthesis and degradation is required for normal morphogenesis and maintenance of tissue architecture. A disbalance in the extracellular matrix turnover either by decreased matrix synthesis and/or increased degradation leads to less than normal extracellular matrix in the leading to cardiac dilatation or even rupture [21].

Myocardial ECM can be broadly divided into three components: (i) the fibrillar structure that is comprised of structural proteins (primarily collagen types I and III); (ii) the basement membrane that forms an interface between the cardiomyocytes and the interstitial space; and (iii) the nonstructural proteins such as proteoglycans [22]. Human cardiac ECM is composed by the 70% of fibrillar collagens, mainly collagen types I and V. The basement membrane represents the 20%, mainly composed of collagen IV, but with additional proteins such as laminin. Structural ECM comprises 4% of cardiac ECM, which include mainly proteoglycans and fibrous glycoproteins. Matricellular components represents the 3% of cardiac ECM, including collagen VI and fibronectin [23]. Collagen is an essential component of cardiac ECM. Collagen type I is the major collagen representing >85% of total collagen, whereas collagen type III represents 6-11%. A small proportion is represented by collagen type V (2-3%) [24]. The myocardium collagen content is normally ~2–4% from morphometric assessment and the rate of collagen turnover in the normal heart is ~5% per day [25]. During physiological turnover, ECM proteins are degraded by the proteolytic function of matrix metalloproteinases (MMPs) and are replaced by newly synthesized proteins. The function of MMPs is kept under check by their inhibitors, predominantly tissue inhibitor of metalloproteinases (TIMPs). A tightly controlled balance in the function of these two groups of proteins is essential in maintaining the integrity of ECM structure [22]. In response to MI, the process of cardiac remodeling includes angiogenesis, myocyte hypertrophy and fibroblast (CFs) proliferation, which results in increased collagen deposition and alterations in ECM proteins and intracellular hormones, cytokines, matrikines and growth factors. These factors include IL-6, TGF-ß, endothelian-1, TNF-α, fibroblast growth factor (FGF) and angiotensin II (Ang II) [26].

In the fibrotic activities of CFs, the mechanical stretch is transmitted by ECM to the integrins on CFs, which causes the release of active TGF-ß and initiates pro-fibrotic cascades. In fact, the ECM can respond to mechanical stretch by activation of TGF-ß in the absence of cells. In addition, ECM-derived molecules named danger-associated molecular patterns (DAMPs) can activate CFs through toll-like receptors (TLRs) in response to pressure overload, which ultimately causes pro-fibrotic gene expression in CFs. Lastly, matrix stiffening can increase CFs spreading and smooth muscle actin fiber formation and cause an increase in collagen I/III ratio. The change in ECM modifies the signals that cardiac cells receive from their scaffolding environment, leading to changes in gene and protein expression associated with myocyte hypertrophy and contractile dysfunction [25].

1.4.3 Development of Cardiac Fibrosis

Following MI, up to 1 billion cardiac cells die in response to ischemia. The adult mammalian heart has a negligible regenerative capacity after injury and the lost cells are replaced by a fibrotic scar. This is followed by remodeling of the surrounding myocardium and eventually cardiac function impairment. The remodeling process includes thickening (hypertrophy) and stiffening (fibrosis) of the left ventricular wall. Cardiac fibrosis results from the excessive synthesis and accumulation of extracellular matrix (ECM) components (e.g., collagen, fibronectin); it is caused by the activation and the proliferation of CFs and MyoFs, leading to an increase of left ventricle stiffness, impairing contraction, relaxation of the heart and mechano-electric coupling. MyoFs are cells that exhibit characteristics of both fibroblasts and smooth muscle cells and they are not present in healthy myocardium. The most remarkable characteristic of MyoFs is their migratory and contracting phenotype, which results from the expression of contractile proteins such as α-smooth muscle actin (α-SMA) and non-muscle myosin, allowing them to exercise stress on the infarcted area. In the short-term outlook, these pro-fibrotic processes can prevent dilatation and laceration of the ventricular wall, resulting beneficial for cardiac efficiency. However, prolonged activity of MyoFs results in excessive fibrosis and tissue stiffening, impairing cardiac function, increasing the risk of arrhythmia and leading to heart failure (HF) (Figure 2) [27].

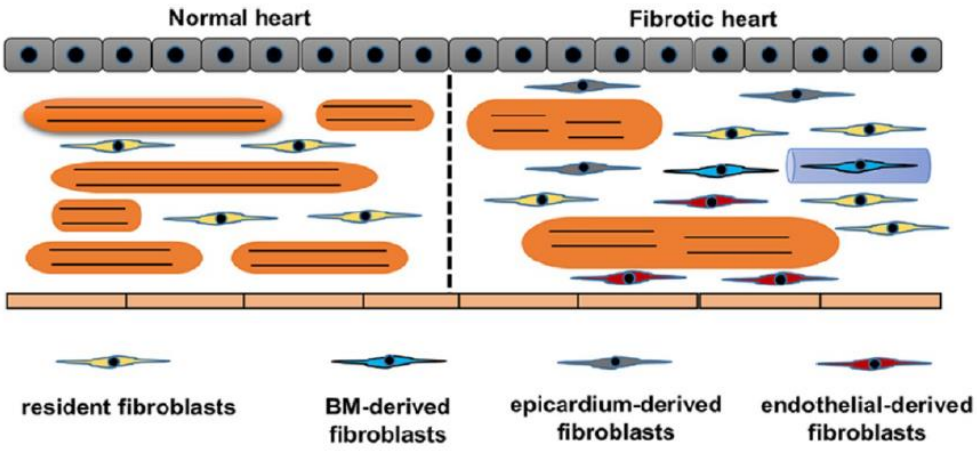

Figure 2. Comparison between healthy and fibrotic tissue morphologies.

The fibrotic response after MI can be classified into two types, namely replacement and reactive fibrosis, both of which are mediated by CF and MyoFs. Replacement fibrosis, i.e., scar formation, is an essential process to prevent rupturing of the ventricular wall after an ischemic insult. Nevertheless, the increased mechanical stress post-MI, added to hormonal and paracrine mediator, induces the expansion of connective tissue in areas remote to the infarction. This reactive fibrosis in the infarct border zone and in the remote uninjured myocardium leads to altered chamber compliance and increased ventricular stiffness, compromising cardiac output [27], [28]. The cellular response to infarction can be divided in three overlapping phases: the inflammatory, the proliferative and the maturation phase (Figure 3). The initial inflammatory phase is triggered by massive necrotic cell death in the infarct area. Marked increases in the cardiac expression of proinflammatory cytokines, namely tumor necrosis factor (TNF-α), interleukin 1 β (IL-1β) and interleukin 6 (IL-6) activate and increase the inflammation. The pro-inflammatory extracellular environment induces cardiac fibroblasts to increase the production of MMP that degrade the ECM allowing immune cell migration into the injured area. Tissue injury activates immune signaling and secretion of chemokines induces leukocyte infiltration into the injured area. The CXC chemokines are known to recruit primarily neutrophils, whereas chemokines from the CC family play a role in recruiting macrophages. These inflammatory cells clear the dead cells and ECM fragments from the infarcted area allowing its repopulation with migrating and proliferating immune cells and, in the latter phase, myofibroblasts. Repression of inflammation, through the increased production of anti-inflammatory mediators such as IL-10 and TGF- β, during the transition from the inflammatory phase to the proliferative phase is associated with the activation of “stop signals” that inhibit inflammation promoting

tissue deposition and angiogenesis. Differentiation and activation of macrophages may stimulate transdifferentiation of MyoFs, the key effector cells in scar formation and the main source of ECM proteins in the healing infarct. At the same time, activation of angiogenic pathways results in the formation of a rich microvascular network necessary to provide oxygen and nutrients to the reparative cells. The end of the proliferative phase may be associated with activation of anti-fibrotic signals, in order to prevent uncontrolled fibrosis. Transition to the maturation phase follows, as extracellular matrix proteins in the infarct are cross-linked, while most fibroblasts and vascular cells in the scar undergo apoptosis. As the scar matures, increased expression of lysyl-oxidase induces cross-linking of the matrix in the infarcted myocardium. Matricellular proteins are cleared and the mature scar, comprised of dense cross-linked collagen, enhances tensile strength of the infarct, increasing passive stiffness and contributing to diastolic dysfunction. In the mature scar, deprivation of growth factors, stress-shielding and removal of matricellular proteins result in apoptotic death of most MyoFs and vascular cells [28], [29].

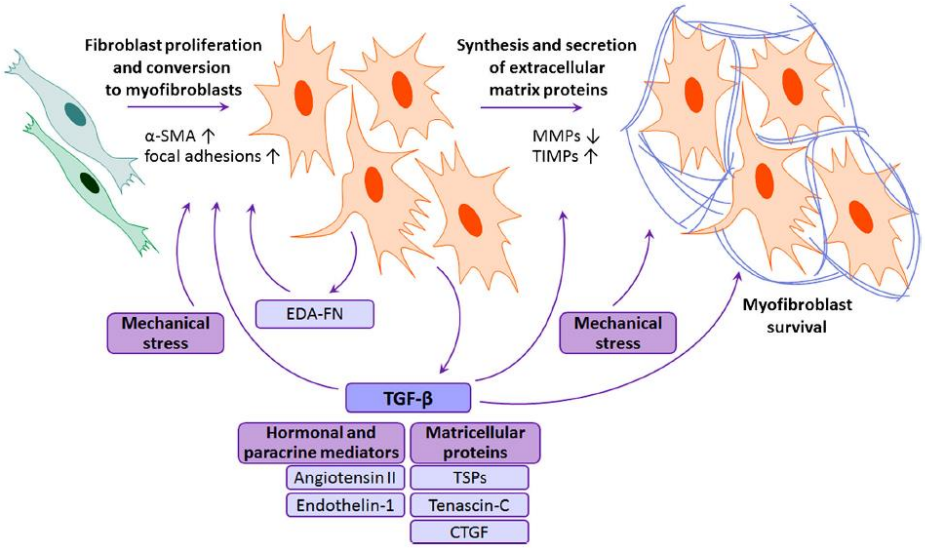

Figure 3. Central pro-fibrotic signaling factors.

1.4.4 Cardiac Fibroblasts Differentiation into Myofibroblasts

Myofibroblasts (MyoFs) are phenotypically modulated fibroblasts that accumulate in sites of injury and combine ultrastructural and phenotypic characteristics of smooth muscle cells, acquired through formation of contractile stress fibers, with an extensive endoplasmic reticulum, a feature of synthetically active fibroblasts. Myofibroblasts derive from multiple sources (Figure 4). In addition to pre-existing local fibroblasts that can differentiate into

myofibroblasts, epithelial and endothelial cells can adopt a myofibroblasts phenotype through the processes of epithelial-mesenchymal transition and endothelial-mesenchymal transition, respectively.

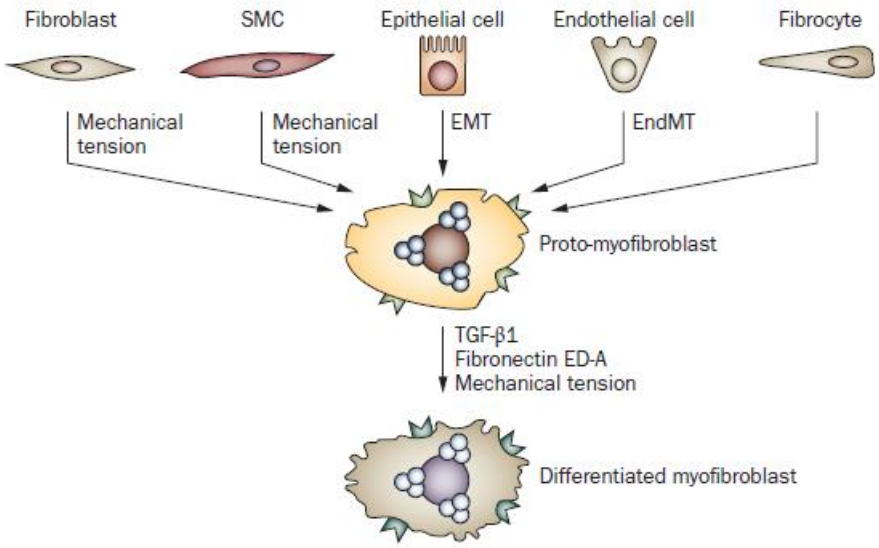

Figure 4. Myofibroblasts precursors and characteristics

Quiescent cardiac fibroblasts don't exhibit actin-associated cell-cell and cell-matrix contacts and don't secrete significant amounts of matrix proteins. Cardiac fibroblasts differentiation into myofibroblasts is a hallmark of the cardiac fibrotic response; incorporation of α-SMA into the stress fibers is a characteristic of differentiated myofibroblasts and significantly increases fibroblasts contractile activity. An important stimulus for the phenotypic transition of a fibroblast to a myofibroblast is a change in the mechanical microenvironment. In an uninjured tissue, fibroblasts are generally protected from stress by the crosslinked ECM framework. As a consequence of Cardiac injury there is a loss of architectural integrity and fibroblasts exposed to mechanical stress become proto-myofibroblasts. Proto-myofibroblasts are characterized by the presence of stress fibers that contain cytoplasmic β-actin and γ-actin. Subsequent exposure to TFG-β1, mainly produced by cardiac fibroblasts, and the ED-A splice variant of fibronectin result in the differentiation of proto-myofibroblasts into myofibroblasts (Figure 5). When the damaged ECM has been reconstructed, the repaired tissue may be able to partially take over the mechanical load. although the myofibroblasts may persist for many years, some myofibroblasts may be removed by apoptosis. The from mechanical stress is a potent promoter of myofibroblast apoptosis. Nevertheless, activation of fibroblasts and inflammatory cells may

persist in the infarct border zone and in the remote remodeling myocardium, as pressure and volume loads may provide stimulatory signals, causing the progression of pathological cardiac fibrosis [12], [29], [30].

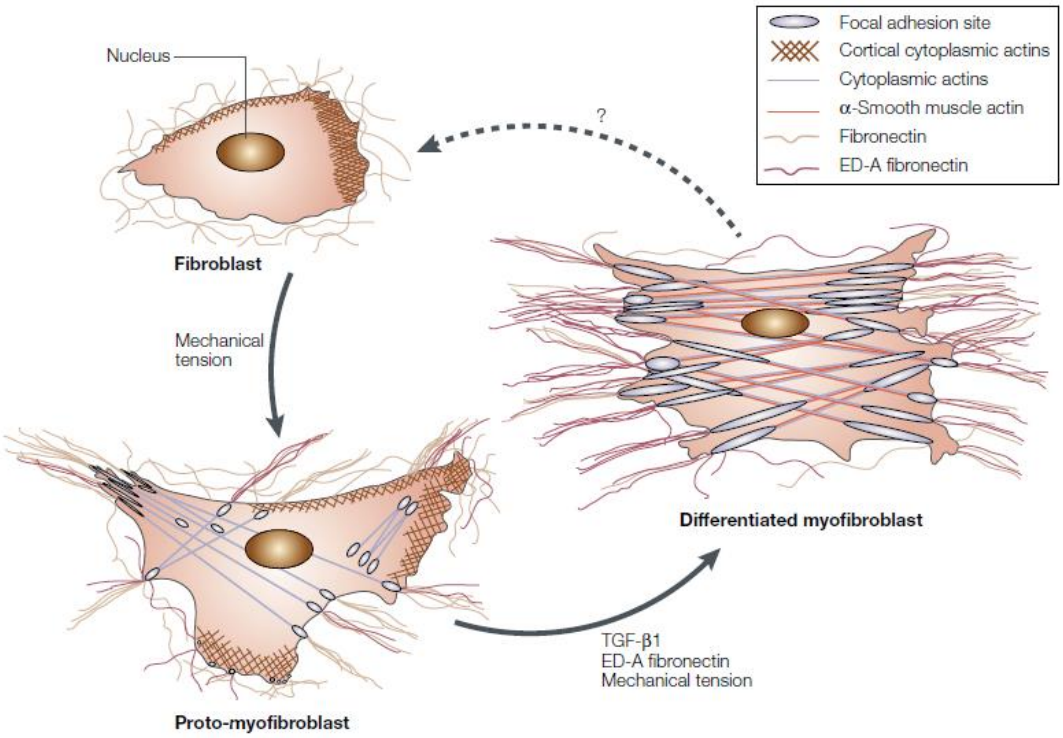

Figure 5. Myofibroblasts precursors and characteristics.

1.4.5 Myocardial Repair

The human heart cannot regenerate significantly because adult cardiac myocytes are terminally differentiated and cannot replicate after injury. Cell-based cardiac repair aims to correct the cause of heart failure's symptoms, that is the injured heart's inability to adequately pump blood due to insufficient muscle mass. Many strategies have been pursued to restore heart function involve repopulating the heart with exogenously delivered cells, either by direct injection or intravascular delivery. The first approach focuses on repopulation of the injured myocardium by transplantation of healthy cells. Several cell types were tested to replace necrotic tissue, such as fetal cardiomyocytes and skeletal myoblasts. These cells shown limited success in restoring damaged tissues and improving cardiac function because of cell death occurring after engraftment and inability of engrafted cells to differentiate and integrate within the host myocardium; hence, electromechanical coupling doesn't occur after in vivo grafting. An

alternative different approach includes mobilization of progenitor or stem cells to the damaged area or stimulation of a regenerative program within the organ. According to some studies, the use of bone marrow mononuclear stem cells can improve the condition of injured heart by regeneration of the cells, it was found that 68% of the cells had regenerated thus showing the usefulness of bone marrow derived stem cells. The benefit of using bone marrow derived stem cells is that they can be derived from the patient, eliminating the possibility of immune response. Embryonic stem cells are used due to their potential to develop into many specialized cell types. However, their application is limited due to ethical and legal issues, but mainly due to the high risk of teratoma formation. Another alternative to repair the infarcted heart is the use of cardiac resident stem cells, they can be induced to develop into cardiac muscle and vascular tissue [31]–[33].

1.5 Tissue Engineering

Tissue engineering is an emerging interdisciplinary field that applies the knowledge of bioengineering, the life sciences, and the clinical sciences in solving the critical medical problems of tissue loss and organ failure. The goal of tissue engineering is to repair or replace the damaged organ or tissue by delivering functional cells, supporting scaffolds, growth factors and signal molecules or DNA encoding these molecules to injured tissues. It applies the principles of bioengineering and life sciences to investigate structure-function relationships in normal and pathological tissues and to develop biological constructs in order to restore, maintain or enhance tissue and organ function [34]. Engineered tissues have the potential to reduce the need for organ replacement and could support the development of new drugs for many diseases. Biologic tissues consist of cells, extracellular matrix (ECM), and the signaling system. The engineered tissue is a triad mimicking the three basic components of the biological tissues (Figure 6) .In order to engineer living tissues *in vitro*, cultured cells are coaxed to grow in three-dimensional (3D) bioactive degradable scaffolds that provide physical and chemical stimuli to guide cells differentiation and assembly into 3D tissues. To achieve successful regeneration of damaged organs or tissues several critical elements should be considered, including the biomaterial scaffold for 3D culture, a relevant selection of cells, that can be differentiated into specific cell types and the presence of appropriate signals, such as biophysical cues and chemical mediators that coordinate cellular activities. There are three principal therapeutic strategies to treat injured tissues in patients: (i) implantation of freshly isolated or cultured cells; (ii) implantation of tissues assembled in vitro from cells and scaffolds

(*in vitro* tissue engineering) ; and (iii) in situ tissue regeneration (*in vivo* tissue engineering). Focusing on cardiac tissue engineering, cardiac cell–polymer constructs could be used as a 3D model for *in vitro* physiological and pharmacological studies and eventually to repair damaged heart tissue *in vivo*. *In vivo* cardiac tissue engineering strategies includes cell seeded scaffold implantation, unseeded scaffold implantation and recruiting endogenous cells, injectable scaffold with or without cells or promotion healing and self-repair by delivery of active molecules. Another valid alternative is represented by the cell–polymer–bioreactor model system that allows control over *in vitro* culture conditions. *In vitro* strategies include engineering cardiac grafts development from cell-seeded scaffold or biomaterial gel, or creation of cell films from cardiac cells and biomaterial sheet. Although *in vitro* approaches provides good control on construct shape, size, cell sources and development, it is limited by the ability to create robust constructs and the risk of tissue necrosis after transplantation. On the other hand, *in vivo* approach aims to create replacement tissue in the natural milieu, it is simpler but poor control on graft development is one of the most important limiting factors. In conclusion, the increasingly intimate combination of engineering and biology offers the prospect of sophisticated physiological in vitro models of many different human tissues. These physiological surrogates will ultimately allow major advances in prevention, diagnosis, and molecular treatment of diseases [31], [35], [36].

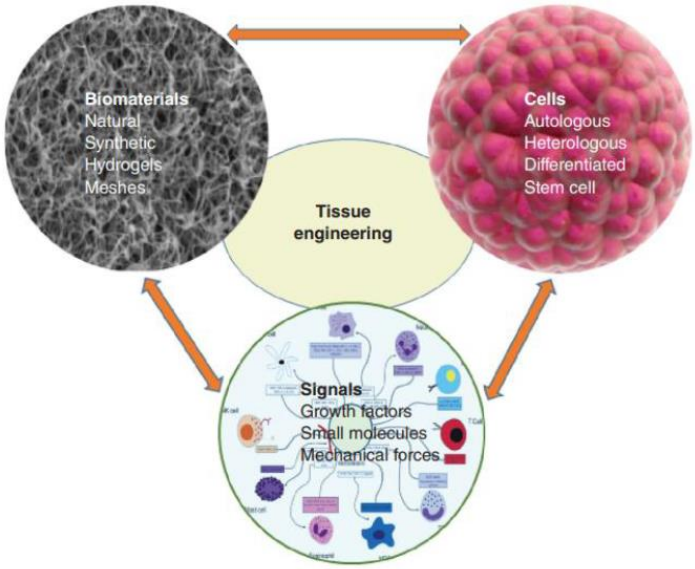

Figure 6. The tissue engineering Triad [37].

1.6 *In vitro* models for cardiac tissue engineering

For decades, the ultimate goal of biomedical research has been to understand the molecular basis of human disease in order to develop new and more effective models of diagnosis, prevention or therapeutic intervention. Most commonly, animals, such as transgenic mice, are used as models of human disease. Although many of these animal models reconstitute disease manifestations and phenotypes that are similar to those observed in humans, the underlying molecular mechanisms can differ greatly between mice and humans. For this reason, a range of new *in vitro* applications, such as safety pharmacology and creating disease models suitable for drug discovery, are being considered, with the goal of translating the laboratory research to treatments for patients. In this case, the engineered tissue is not a medicinal product, but the vehicle for testing treatments. In this application of tissue engineering, the tissues are small enough to avoid diffusional constraints for oxygen supply and the regulatory requirements are minimal. The three-dimensional (3D) tissue models are expected to respond exactly as a native tissue. Moreover, such models can recapitulate certain physiological functions and be used in early-stage research to investigate the efficiency, safety and mood of action of therapeutic agents. Instead of attempting to mimic the complexity of the whole organ, the goal is to replicate the tissue specific architecture so that it recapitulates a subset of most relevant physiological function of the tissue of interest (Figure 7) [37], [38].

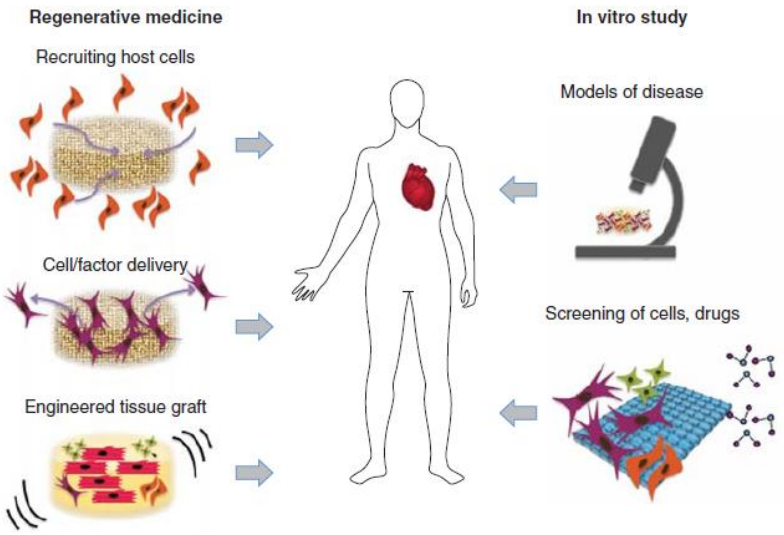

Figure 7. Myocardial tissue engineering for modeling disease and high-throughput platforms for screening of drugs and therapeutic targets.

A range of innovative *in vitro* 3D-culture systems for cardiac disease modeling have been developed and have been utilized for drug testing and pharmacology studies. In this field, tissue engineered models of cardiac fibrosis are indispensable for advancements in the field of anti-fibrotic therapeutics in order to treat heart failure after myocardial infarction. Although conventional monolayer (2D) cell culture methods have provided valuable insight into cardiac tissue physiology, they don't adequately represent the human in vivo (3D) myocardial tissue. Conventional cell culture strategies are associated with major differences in structural and functional properties compared to native myocardium. These differences are mostly characterized by (i) the lack of native-like biochemical, electrophysiological, and mechanical cell–ECM and cell–cell interactions, (ii) the differences in dynamic *in vivo* like conditions such as fluid flow and shear stress, and (iii) variations in molecular expression profiles, cell morphology and structural microarchitecture. On the other hand, 3D models are characterized by establishment of adhesion complexes and tissue polarity and by changes in cytoskeletal structure and cell volume that are significantly different from those found in cells cultured as monolayers [39], [40]. Several studies have been focused on modeling healthy and infarcted myocardium, culturing cardiac cells on different scaffolds. French et al. demonstrated elevated gene expression of early and late cardiomyocyte markers in cardiac progenitor cells on porcine myocardial matrix . They found that proliferation, viability and adhesion also increased. These shifts were not produced on adipose ECM coatings, suggesting the tissue specific ECM provided a more ideal cell environment. Greater gene expression of ECM, MMPs and adhesion proteins also suggested induced remodeling of the microenvironment. Sullivan et al. utilized rat myocardial matrix-polyacrylamide gels mimicking the healthy and infarct cardiac microenvironment in order to investigate the effects on the mesenchymal stem cells phenotype. Conditions representative of the diseased conditions, shifted expression of early cardiac markers and secretion of certain growth factors was increased, supporting hypotheses that therapeutic effects of stem cell treatment are achieved by a reparative paracrine mechanism [41]. In hybrid porcine myocardial matrix-collagen scaffolds, Duan et al. encapsulated human embryonic stem cells (hESCs) embryoid bodies and compared their differentiation toward a cardiomyocyte phenotype to protocols with pure collagen gels and additives mimicking early cardiac factors patterns. Gels with higher percentages of ECM had both significantly greater and more prolonged gene expression of cardiomyocyte markers compared to both growth factor regimens and pure collagen gels. Beating populations, contraction amplitudes, and gap junction organization were also increased [42]. Basing on the idea that a hydrogel perfectly mimics native cardiac ECM and provides a physiological microenvironment for the cells, Freytes et al.

described a method for making 3D hydrogels scaffolds from decellularized cardiac ECM with additional collagen type I. They found that native cardiac ECM has a positive effect on the differentiation and maturation of hESC to CMs. Hydrogels with high cardiac ECM content showed an elevated expression of cardiac markers and it was observed an improvement in contractile function and maturation of the cardiac differentiated cells. Although this platform was created by using only hESCs, it could potentially be used to create a 3D model with both CMs and CFs to study MyoFs differentiation in the presence of differentiated and contractile CMs [39]. Hjortnaes et al. proposed a hydrogel platform composed of photo-crosslinkable versions of native valvular extracellular matrix components (HAMA and GelMA) as a 3D culture system to study valvular interstitial cell (VIC) phenotypic changes. Their results showed that VIC myofibroblast-like differentiation occurs spontaneously in mechanically soft GelMA hydrogels, but in HAMA-GelMA hybrid hydrogels it requires exogenous delivery of TGF-β1. This study demonstrated that a hybrid hydrogel platform can be used to maintain a quiescent VIC phenotype [43]. A later study carried out by Gartner et al. suggested that HCF-laden GelMa is a suitable model to mimic cardiac fibrosis, thereby providing a platform for pathophysiological studies and drug testing. Using this model, they were able to demonstrate the anti-fibrotic effects of cardiac progenitor cells (CPC) *in vitro,* also revealing an important role for continuous cross-talk between CPC and HCF [40]. In their work, Saini et al developed 3D cardiac microtissues embedded with the co-culture of CM and CF using GelMA hydrogel controlling precisely the geometrical features of the microtissues. They observed enhanced cytoskeletal organization, specific cardiac protein expression, and synchronous contraction of the co-culture of the cells compared to the monoculture condition regardless of construct geometries. Furthermore among the co-culture conditions, increasing the number of CM resulted in a significantly enhanced beating frequency. These findings can be used in engineering the next generation of cardiac tissue substitutes for regenerative medicine and disease modeling application [44]. In another study of Deng et al. a 3D CF tissue was engineered by encapsulating isolated rat adult CF in a collagen-based hydrogel. The aim of the study was to measure the effect of a thrombin receptor inhibitor (PAR1) on cardiac fibrosis. By adding thrombin, they observed that the tissue stiffness increased significantly, which then was reduced after incubation with PAR1 inhibitor. The study of Deng et al. indicates the importance of a cardiac fibrosis model in the identification of drug targets as well as the identification of pathophysiological processes that play a key role in cardiac fibrosis and ventricular remodeling [39]. All the models cited above have in common the use of natural polymers as constituent, on the contrary the last work presented make use of a synthetic polymer as building constituent of

the model. Poobalarahi et al. developed a 3D culture system using primary cardiac fibroblasts seeded into a nylon mesh (3DTC) that allows to interconvert between myofibroblast and fibroblast phenotypes. They have found that CF in 3DTC convert to MyoFs through interaction with the scaffold and that stretch induces phenotypic conversion to fibroblasts with a concomitant reduction in collagen production [45].

1.6.1 Cell sources for *in vitro* cardiac tissue models

An ideal *in vitro* cardiac tissue model should accurately recapitulate the physiological or pathological conditions of the human heart, including 3D anisotropic tissue structure, orientation of the ECM network, vascularization and circulation. Human cardiovascular conditions *in vitro* can be achieved by developing engineered physiologically relevant 3D models by embedding cells in biomaterial matrices or microfabricated devices.

In the adult human heart, CMs account for about 70% of the heart volume, but they represent only about the 30% of the total cell number. Therefore, identifying the optimal source of beating CMs is the first step in the development of an *in vitro* cardiac tissue model. Early cardiac tissue models depended on immortalized human cell lines or primary cells isolated from multiple species. Primary CMs isolated from embryonic chicken and neonatal mice and rats were the most common cell sources for cardiac models. The increased awareness that animal cell-based models cannot recapitulate human physiology in a reliable way has led to the development of more sophisticated cells to build tissue models. The advancement of stem cell biology played a key role in the development of *in vitro* cardiac tissue models that employ differentiated pluripotent stem and progenitor cells. Originally, mesenchymal stem cells (MSCs) were used for cardiac tissue models to investigate their beneficial effects on damaged cardiac tissues, either through transdifferentiation or paracrine signaling. However, MSCs suboptimal capability for cardiac differentiation has limited their use in this field. For better recapitulation of heart's physiology and pathology, nowadays *in vitro* cardiac models focus on human pluripotent stem cells, including human embryonic stem cells (hESCs), human pluripotent stem cells (hPSCs) and human induced pluripotent stem cells (hiPSCs). CMs differentiation *in vitro* differ considerably from cells isolated from a mature human heart, because of the absence of humoral factors and organized mechanical and electrical stress. In general, many of the features of hPSC-CMs are reminiscent of normal fetal cells. hPSC-CMs are spontaneously beating cells co-expressing atrial-, ventricular-, and nodal- markers, with unorganized sarcomeres, immature mitochondria and an expression profile different from adult CMs. Despite all the discussed

limitations, hPSC differentiation remains a powerful method to model *in vitro* cardiac disease because of the capacity of these cells to give rise to terminally differentiated stable cardiac cells [46]. In some studies, contracting CMs were generated from hiPSC through co-culture with mouse endoderm-like cells (END2). One key area of research that needs to be addressed prior to full-scale use of iPSCs for cardiac drug screening and development is the maturity of CMs. CM maturation *in vivo* is regulated by diverse factors, including topographical, electrical, mechanical, chemical and cellular interaction cues. However, hiPSC-CMs *in vitro* retain a relatively immature phenotype and exhibit relatively small size, reduced electrical excitability and impaired excitation-contraction coupling. Currently, efforts focus on dissecting the external cues (chemical, physical, electrical), deciphering signaling pathways and using this information to accelerate the maturation process. Engineering methods are playing a crucial role to stimulate the *in vitro* processing of hiPSC-CMs maturation by providing relevant environmental motifs, such as morphology, external electrical stimulation, mechanical loading and extracellular matrices [38], [47], [48]. Basing on all the advances cited above there are new possibilities for disease modeling of cardiac fibrosis providing high availability and relatively low cost compared to animal models. Most of the current *in vitro* models of cardiac tissue contain only CMs and lack other cell types found in the human heart. Therefore, there is a need for an *in vitro* human cardiac fibrosis model that possesses the physiological relevant cell combination and can mimic the 3D nature of native cardiac tissue. To this end Lee et al. found that using CMs and MSCs, both differentiated from the same hESC line, MSCs could provide a major precursor population to generate CF, which mediate scar formation during fibrosis [49]. In another study focused on hiPSCs, Zhang et al. demonstrated that it was possible to generate quiescent cardiac fibroblasts form hiPSCs, that could recapitulate most of the fundamental biological features of primary CFs. They was further demonstrated that hiPSC-CFs could be used as an *in vitro* model to explore the underlying mechanism of cardiac fibrosis and to screen drugs with pro-or anti-fibrosis potential [50].

1.6.2 Biomaterials for *in vitro* cardiac tissue models

Native heart matrix is a highly ordered anisotropic structure that supports densely packed CMs and supporting cells. Engineering a 3D cardiac tissue with physiologically relevant microenvironment and cell morphology presents a significant challenge for *in vitro* cardiac modeling. Biomaterials play a key role in creating 3D tissue models, scaffolds should provide a 3D environment for cells to attach, interact with each other, transmit load and conduct

electrical signals. A suitable scaffold for cardiac tissue engineering has the capacity to induce alignment and provide appropriate stiffness for the cells to generate physiological force. Moreover, highly ordered anisotropic layers within native myocardium are critical for alignment of CMs and the transduction of mechanical and electrical signals. For normal function, cardiac cells need a matrix with cardiac-like molecular composition, structure, and mechanical properties. Two broad classes of cardiac tissue engineering scaffolds are natural and synthetic materials. Natural materials include collagen, hyaluronic acid (HA), Matrigel, fibrin, elastin, gelatin, alginate and decellularized heart matrix. They have the advantage to provide signals to cells by surface receptor interactions, but they are difficult to process without disrupting important hierarchical structures. Hydrogels formed from natural materials are particularly suitable for cardiac tissue engineering applications because their mechanical properties are tunable and they can be adjusted to values inherent to native heart matrix. However, the poorly defined chemical composition and batch-to batch variability have limited the application of natural polymers in certain cases. In addition, their mechanical properties are not always sufficient to support many tissue types. Some attempts have been made in order to overcome such mechanical deficiency. For example, hybrid system were generated to enhance the mechanical properties of natural polymers: semi-interpenetrating networks of photocrosslinkable hyaluronic acid (MeHA) and collagen have been fabricated to achieve better mechanical properties than collagen or MeHA alone. Chemical modifications can also be considered in order to tune the mechanical strength of natural polymers. For example, the varied modification degree of methacryloyl-substituted gelatin (GelMA) can be used to obtain scaffolds with desired mechanical properties that are suitable for cardiac tissue engineering applications [39]. Several groups have used biological tissues ad scaffold, for example decellularized heart tissue. Decellularization of tissues removes all cellular elements, leaving an intact and functional ECM. Thin sheets of decellularized human heart matrix were an excellent substrate for *in vitro* cultivation of cardiac cells. Such scaffolds can provide a combination of local control and long-range signaling. Synthetic biomaterials provide an attractive alternative to natural materials, as it is possible to control the entire synthesis process as well as the materials mechanical properties, topography and structure. A number of synthetic polymers have been used to create 3D cardiac scaffold for *in vitro* models. Synthetic scaffolds must recapitulate the native 3D hierarchical fibrillar structure, possess biomimetic surface properties and demonstrate mechanical integrity. The most frequently used synthetic polymers for cardiac tissue engineering are polyurethane, poly-caprolactone (PCL), polylactic acid (PLA), polyglycolic acid (PGA) and their copolymers. Synthetic biomaterials can be readily

customized, but may be limited in functional cellular interaction and therefore they are often modified to incorporate adhesion peptides or release biological molecules. An excellent synthetic material for cardiac tissue engineering is the poly(glycerol sebacate) (PGS). PGS has been used in cardiac tissue applications because of its high and controllable elasticity and stiffness. This material was used to fabricate scaffold in the form of an honeycomb with anisotropic structure and biochemical properties of native cardiac muscle. It has been demonstrated that this type of scaffold induced cell alignment, coupling and a direction-dependent contractile behavior. In general, cell alignment can be obtained with electrospun nanofiber-based scaffolds, which provide flexible matrices and topographic properties offering support and guidance for the CMs. Electrospun 3D scaffold with aligned nanofibers using synthetic polymers successfully mimic the structure and orientation of native ECM in the myocardium and help CMs self-organize with anisotropic structure. However, the micron scale porosity of these scaffold limits call infiltration into the matrix and thereby the creation of a 3D tissue.

The scaffold is a key component of almost all tissue-engineered systems as it determines interactions between the cells and their environment. Specialized scaffolds are now available that guide cell alignment, improve mass transport and provide the mechanical properties necessary for the formation of cardiac tissues in vitro. These findings collectively suggest that 3D tissue engineered models with defined cellular microenvironments hold great promise for high-content drug screening and cardiotoxicity testing [38], [47], [51].

1.6.3 *In vitro* stimulation

Cardiac tissue is characterized by being dynamic and contractile, imparting the important role of biomechanical and biochemical cues in the regulation of physiological activity or pathological remodeling. The alteration of biochemical and biomechanical microenvironments in cardiac tissue determinates the fate of CFs fibrotic remodeling. Since the mechanism by which fibrosis occurs is unclear, clarifying the underlying crosstalk between biochemical and biomechanical cues is important for the development of new therapeutic strategies for cardiac fibrosis. In terms of biochemical cues, many soluble cytokines such as TGF-β, angiotensin II, interleukin-6, endothelin-1 and basic fibroblast growth factor have been implicated in myofibroblast activation. Among which, TGF-β plays the major role in the activation of myofibroblasts promoting the expression of α-SMA and synthesis of extra domain-A (ED-A) fibronectin and it is often used as a unique triggering factor to mimic a fibrotic environment *in*

vitro. In addition, it is important to considerate many biomechanical factors, such as ECM stiffness and mechanical strain, that are crucial in the regulation of heart fibrosis and pathological remodeling. *In vitro*, fibroblast/myofibroblasts are cultured and regulated by controlled biomechanical conditions [52]. Many studies showed that substrate stiffness alone can regulate the fate of fibroblasts by mainly promoting fiber formation (e.g. expression of stress fibers), while external mechanical stretching regulates instead expression of α-SMA and types I and II collagen deposition. However, in 2D culture environments, the effect of external static stretching depends on the chosen substrate stiffness and it seemed to induce fibrotic gene and protein expression only when a scar-like substrate (~30 kPa) is used. Starting from the muscle-like stiffness range (3–10 kPa), the effects of static mechanical stretching on pro-fibrotic switch were less evident. Although 2D in vitro models of fibrosis offer a good control over culture substrate stiffness, they cannot mimic the complexity of the native 3D environment characterized by cell–cell and cell–matrix interactions. To this end, microfluidic technologies have been investigated to enable the development of advanced cardiac models by integrating key environmental features within cardiac cell culture systems, such as cyclic mechanical strain and the supplementation of specifical biochemical factors (TGF-β1). The results of the use of microfluidic platforms showed that the supplementation of exogenous TGF-β1, both alone and in combination with cyclic mechanical stimulation, contributed to an increase in the final cell density within the model and in the fibroblast proliferative activity, However, also cyclic mechanical stimulation alone was shown to be capable of triggering fibroblast proliferation, if compared to the static control without TGF-β1 supplementation. Taken together, these observations suggested that both TGF-β1 supplementation and cyclic mechanical loading are effective in stimulating *in vitro* the recapitulation of the early proliferative stage of wound healing. In conclusion, integrating 3D culture, microfabrication and biomechanical cues regarding fibrotic progress could be useful to study the mechanical regulation of myofibroblast activation and fibrotic remodeling, especially to uncover the strain-response relationship of mechanical cues and CFs phenotypic remodeling [52]–[54].

1.6.4 Biomimetic Coatings for *in vitro* cardiac fibrosis models

Cardiac tissue engineering and regenerative medicine rely on biomaterial scaffolds to support cell attachment, proliferation, differentiation *in vitro.* Mimicking the best natural scaffold, the extracellular matrix (ECM), represents a good strategy to reproduce biochemical signals in a 3D environment. Cells integrate with the ECM *in vivo* as a physiologic mechanism involving

bi-directional interaction between the intracellular environment and the surrounding ECM itself, through cell-surface receptors. These interactions induce specific behaviors and differentiation of individual cells. Recent strategies in the developing of tissue engineered biomaterials have focused on changes to the surface characteristics of the scaffolds to control cell response. Scaffold of aliphatic polyesters such as poly(L-lactic acid) (PLA), poly(L-lactic-co-glycolic acid) (PLGA) and poly(ε-caprolactone) (PCL) are often used in tissue engineering because they provide tunable properties such as ease of manufacturing, good mechanical properties and non-toxic degradation products. However, cell-surface interactions are limited on these materials by their smooth post-fabrication surfaces, hydrophobicity and lack of biochemical binding sites. To overcome these limits, biomimetic surface modification techniques have been developed to unite the consistency and the mechanical properties of synthetic polymers with the cell-signaling potential found in native tissues [55], [56]. In the field of cardiac tissue engineering, many researches have used ECM proteins to make coatings on synthetic polymers in order to provide a more *in vivo* like environment. For instance, PGA scaffolds coated with laminin were found to increase cell size and induce a change in the electrical properties of a membrane populated with cardiomyocytes. Other studies demonstrated that laminin improves the adhesion and alignment of cardiomyocytes [51]. Schenke-Layland et al. used collagen type IV coatings to induce iPSCs to differentiate into functional cells of the cardiovascular and hematopoietic lineage [57]. Cardiomyocytes have many different surface integrins which allow attachment to various ECM proteins. A few studies have shown that cardiomyocytes have demonstrated good attachment to polymers modified with collagen type I , laminin or fibronectin and that they exhibit spontaneous contractility, suggesting that these coatings are able to promote cells adhesion in 2D cultures and to influence cardiac morphology [58], [59]. Moreover, scaffold surfaces, modified with ECM molecules, are shown to modulate cellular activities of fibroblasts that modulates myo-fibrillogenesis. For example, the coating of PLGA with ECM has been found to upregulate property of cardiac markers [60]. As an alternative strategy, decellularized matrix (DM) coatings were investigated to confer bioactivity to synthetic substrates through the addition of a complex, physiologically relevant ECM to biomaterial surfaces. DM coatings are produced by first culturing matrix-depositing cells on a substrate, followed by the removal of those cells such that the underlying matrix remains intact. Subsequently, cultured cell populations are then able to directly interact with residual ECMs. The successful application of DM coatings to 3D constructs currently requires customized perfusion flow bioreactors to minimize DM heterogeneity resulting from poor oxygen and nutrient diffusion to matrix-deposing cells. This technique may be costly and time consuming

in the eventual scale up of DM coatings to customized materials of differing geometries. For this reason novel approaches are being investigated, for example DMs deposited on standard tissue culture plastic (TCP) can be removed, solubilized and transferred to alternate substrates, while retaining cell-instructive properties [61].

1.7 Biomimetic Coatings Validation: Quartz Crystal Microbalance (QCM)

The quartz crystal microbalance (QCM) is a nanogram sensitive technique that utilized acoustic waves generated by oscillating a piezoelectric, single crystal quartz plate to measure mass. The basis of QCM operation relates to quartz's inherent property of piezoelectricity. By applying alternating electric fields to quartz an alternating expansion and contraction of the crystal lattice is induced. In the most common QCMs a circular piece of quartz is sandwiched between two metal electrodes. Resonance is excited when a sufficient AC voltage is applied with a frequency close to the resonant frequency (f_0) of the particular crystal. The resonant condition of the QCM occurs when the standing wave produced by the alternating expansion and contraction is an odd integer of the thickness of the quartz plate. Resonant frequencies of typical QCMs are on the order of MHz and the tradeoff between frequency (relating to sensitivity) and the thickness (relating to usability) of QCMs is that the higher the resonant frequency the thinner the crystal. QCM is used to observe and quantify real-time molecular absorption processes on a solid-liquid interfaces. The absorption of molecule or particles on the sensor surface causes a change in the resonant frequency (Δf) of the quartz crystal sensor. Frequency variation is detected using acoustic waves generated by the oscillation of a piezoelectric crystal, following the application of an alternating electric field (Figure 8). In addition, QCM-D provides information on the stiffness of an absorbed layer by monitoring dissipation (ΔD). Δf essentially measures changes in the mass attached to the sensor surface (generally golden sensor), while ΔD measures properties related to the viscoelastic properties of the adlayer [62]–[64].

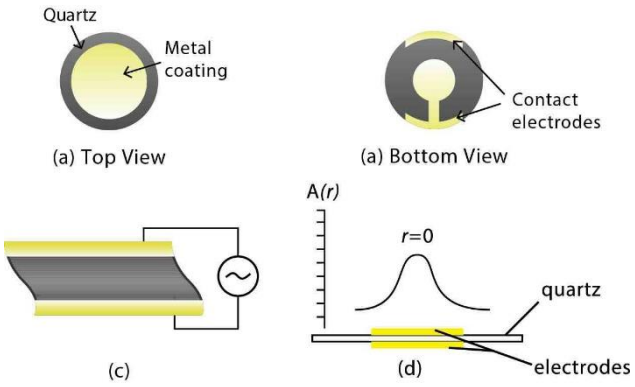

Figure 8. Golden sensor schematic rapresentation.

When the deposited material is viscous or soft, it doesn't follow the sensor oscillation perfectly, this leads to internal friction (due to deformation) in the adlayer and thus to dissipation. This mass is the dynamic mass and not the rest mass. The more viscous the material the more the oscillation will induce deformation and thus the coupled mass will deviate more and more form the rest mass. Therefore, using the dissipation parameter it is possible to fully characterize the adsorption of viscoelastic materials. In practical biomolecular applications the dissipation parameters and the subsequently extracted viscoelastic parameters are critical for many applications, such as cellular adsorption applications.

1.8 Direct reprogramming of cardiac fibroblasts into myocytes

Heart disease is a leading cause of adult and childhood mortality worldwide. Because human hearts have low regenerative capacity following injury, all heart injuries heal by scar formation, potentially leading to cardiac remodeling and heart failure. Cardiac fibroblasts (CF) represent a significant fraction of the non-myocyte cell population in the heart and they are crucial in pathological cardiac remodeling, for this reason they are attractive therapeutic targets for cardiac repair. A major goal for the treatment of heart tissue damaged by cardiac injury is to develop strategies that restore healthy heart muscle through the regeneration and repair pf damaged myocardium. The discovery of induced pluripotent stem cells (iPSCs), in 2006, inspired new approaches for generating specific cell types by introducing combinations of lineage-specific transcription factors. Recent advances have established that CFs can be directly reprogrammed into cardiac myocytes by introducing combinations of lineage-significant transcription factors or microRNAs (miRNAs) without first becoming stem/progenitor cells.

In the context of myocardial infarction (MI), researchers adopted an autologous *in vivo* strategy consisting in the delivery of a cocktail of reprogramming mediators directly into the border zone adjacent to the injured myocardium and thereby inducing fibroblasts to reprogram into cardiac muscle. This approach would be expected to lead both a reduction on scar formation and an overall improvement in contractility (Figure 9) [65], [66].

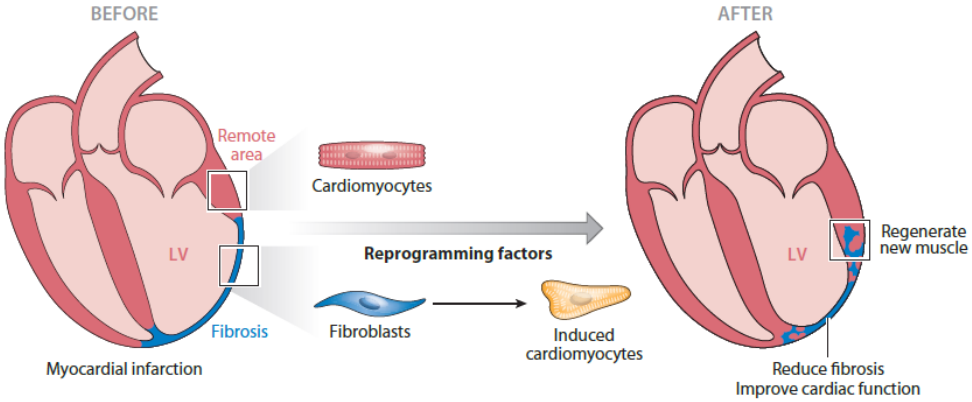

Figure 9. Direct reprogramming of cardiac fibroblasts into cardiomyocytes in situ.

An important question for regenerative purposed is whether a direct reprogramming strategy can convert adult fibroblasts into fully functional cardiomyocytes. To address this, Song et al. determined the optimal combination of the cardiac transcription factors necessary and sufficient for reprogramming of tail-tip fibroblasts (TTFs) into functional cardiomyocytes. In addition, miRNAs have been widely investigated as such they have numerous targets related to signaling pathways, transcription factors and epigenetic regulation and play important roles in cell fate decisions. The four muscle-specific miRNAs—miR-1, miR-133, miR-208, and miR-499—are abundantly expressed in cardiomyocytes, where they regulate heart development and many aspects of cardiac biology. Jayawardena et al. reported that a combination of these four muscle-specific miRNAs could convert neonatal mouse CFs into cardiomyocyte-like cells *in vitro*. The resulting induced cardiomyocytes (iCM) expressed cardiac proteins and sarcomeric structures and the results suggest that miRNA mimics may be applicable to cardiac reprogramming and may have advantages for clinical applications [66]. Analyzing all the experiments performed, it was found out that the reprogramming efficiencies achieved i*n vivo* was higher than those achieved in vitro, suggesting that some elements of the microenvironment actively influence the process [67]. Comparing *in vivo* and *in vitro* reprogramming, *in vivo*-generated iCMs seem to be more fully reprogrammed, suggesting that secreted proteins, electrical and mechanical stimulation, and cell to cell contact may promote cardiac differentiation and reprogramming. Despite the huge potential of direct cardiac reprogramming technology, many challenges remain. The reprogramming process *in vitro* is inefficient and the molecular mechanism of direct reprogramming is still undefined. Given that the reprogramming factors identified *in vitro*

can be applied *in vivo*, *in vitro* studies can be used as screening platforms for the identifications of key factors to further improve reprogramming efficiencies (Figure 10) [66].

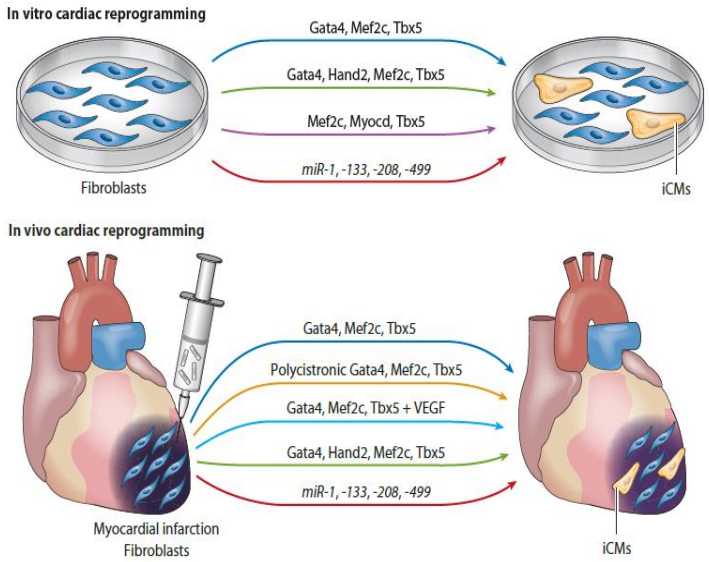

Figure 10. Direct cardiac reprogramming in vitro and in vivo.

1.9 Electrospinning

Electrospinning is a unique and versatile technique that depends on the electrostatic repulsion between surface charges to constantly draw smooth nonwoven fibers from polymer solutions or melts. Considering all the Tissue Engineering techniques, electrospinning is the only method that allows mass production of nanofibers from various polymers, it is simple, cost-effectiveness, versatile, scalable and reliable. [68], [69] Electrospun fibers diameters range from 2 nm to several micrometers. Compared to standard fibers, they offer several advantages such as, an extremely high surface-to-volume ratio, tunable porosity and malleability to conform to a wide variety of size and shapes. Because of these advantages, electrospun nanofibers have been widely investigated in the past several years for use in various applications, such as filtration, optical and chemical sensor and biological scaffold for tissue engineering. An electrospinning system consists of three major components: a high voltage supply, a volumetric pump and a conductive grounded collector (usually a metal screen, plate or rotating mandrel) (Figure 11).Currently, there are two standard electrospinning setups, vertical and horizontal [70].

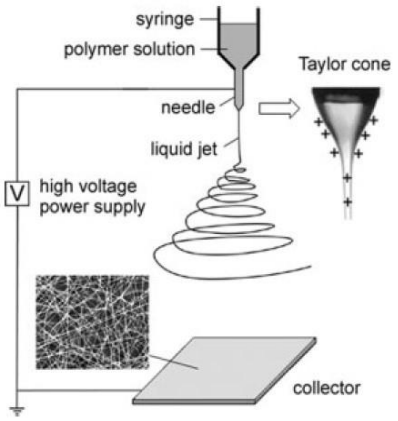

Figure 11. Schematic diagram of set up of vertical electrospinning system.

Direct current (DC) power supplies are usually used for electrospinning although the use of alternating current (AC) potential is also feasible. The spinneret is connected to a syringe in which the polymer solution is hosted. With the use of a volumetric pump, the solution can be fed through the spinneret at a constant and controllable rate. When a high voltage is applied (usually in the range of 1 to 30 kV), the pendent drop of polymer solution at the nozzle of the spinneret will become highly electrified and the induced charges are distributed over the surface. As a result, the drop will experience two major types of electrostatic forces: the electrostatic repulsion between the surface charges and the Coulomb force exerted by the external electric field. Under the action of the electrostatic interactions, the drop will assume a conic shape, originating the Taylor cone. Once the strength of electric field has exceeded a critical value, the electrostatic forces can overcome the surface tension of the polymer solution and thus force the ejection of a liquid jet form the nuzzle. The electrified jet then undergoes a stretching process forming a thin wire. As the liquid jet is continuously elongated the solvent is evaporated and its diameters is reduced. The collector attracts the charged fiber, that it is often deposited as randomly oriented [71]. The morphology and diameter of electrospun fibers depend on a number of processing parameters that include: (i) the intrinsic properties of the solution such as the type of polymer, the conformation of polymer chain, molecular weight, concentration, elasticity, electrical conductivity and the polarity and surface tension of the solvent; and (ii) the operational conditions such as applied voltage, the distance between spinneret and collector and the feeding rate for the polymer solution. In addition, ambient parameters, such as humidity and temperature of the electrospinning chamber may also play an important role. The polymer molecular weight influences solution viscosity, surface tension

and conductivity. In general, easily spinnable polymers have high molecular weight, while polymers with low molecular weight tend to form beads. It exists a minimum concentration below which an “electrospraying” process is stablished (it causes the deposition of particles instead of fibers) and a maximum concentration beyond which it the solution is too viscous to have a continuous process. Surface tension, more likely to be a function of solvent compositions of the solutions, plays a critical role in the electrospinning process and by reducing the surface tension of the solution, fibers can be obtained without beads Generally, the high surface tension inhibits the process because of instability of the jets. Solution conductivity is mainly determined by the polymer type, solvent used, and the availability of ionizable salts. It has been found that with the increase of electrical conductivity of the solution, there is a significant decrease in the diameter of the electrospun nanofibers whereas with low conductivity of the solution, there results insufficient elongation of the jet to produce uniform fiber and beads formation may occur. The selection of the solvent is one of the key factors for the formation of smooth and beadless electrospun nanofiber. Usually, two things need to be considered before selecting the solvent. First, the polymer has to be completely soluble in the chosen solvent. Second, the solvent should have a moderate boiling point. Its boiling point gives an idea about the volatility of a solvent. Generally volatile solvents are fancied as their high evaporation rates encourage the easy evaporation of the solvent from the nanofibers during their flight from the needle tip to collector. However, highly volatile solvents are mostly avoided because their low boiling points and high evaporation rates cause the drying of the jet at the needle tip. This drying will block the needle tip and hence will hinder the electrospinning process. Similarly, less volatile solvents are also avoided because their high boiling points prevent their drying during the nanofiber jet flight. As regard processing parameters, the applied voltage to the solution is a crucial element. A higher voltage caused greater stretching of the solution leading to a reduction in the fiber diameters and also to a rapid solvent evaporation from the fibers. The flow rate of the polymer is another important process parameter as it influences the jet velocity and the material transfer rate. A lower flow rate is suitable as the solvent will get enough time to evaporate. High flow rates result in beaded fibers as the solvent evaporation is uncomplete prior to reaching the collector. One important aspect of the electrospinning process is the type of collector used, it is possible to obtain a random mass of fibers, using a conductive flat plate or advanced collection systems can be used to obtain aligned fibers, such as the rotating cylinder, two parallel metal rods or two rings equidistant from the spinneret parallel to each other. The distance between the tip and the collector has been examined as another approach to control the fiber diameters and morphology. It has been found that a minimum distance is

required to give the fibers sufficient time to dry before reaching the collector, otherwise with lower distances beaded fibers can be observed. Apert from solution and processing parameters, it is important to consider the influence of ambient parameters. It has been found that with increase in temperature, there is a yield of fibers with decreased fiber diameter and this can be explained relating it with a decrease in the viscosity of the polymer solution at increased temperature (Table 1) [70], [72].

Table 1 Electrospinning parameters effect on fiber morphology

Parameters	Effect on fiber morphology
Solution parameters	
Viscosity	Low-beads generation, high-increase in fiber diameter , disappearance of beads.
Polymer concentration	Increase in fiber diameter with increase of concentration.
Molecular weight of polymer	Reduction in the number of beads and droplets with increase of molecular weight.
Conductivity	Decrease in fiber diameter with increase in conductivity.
Surface tension	No conclusive link with fiber morphology, high surface tension results in instability of jets.
Processing parameters	
Applied voltage	Decrease in fiber diameter with increase in voltage.
Distance between tip and collector	Generation of beads with too small and too large distance, minimum distance required for uniform fibers.
Feed rate/Flow rate	Decrease in fiber diameter with decrease in flow rate, generation of beads with too high flow rate.
Ambient parameters	
Humidity	High humidity results in circular pores on the fibers.
Temperature	Increase in temperature results in decrease in fiber diameter.

Electrospinning generates loosely connected 3D porous mats with high porosity and high surface area which can mimic extra cellular matrix structure and therefore makes itself an excellent candidate for use in tissue engineering. Myocardial tissue shows a hierarchical structure with aligned fibrous cells embedded into 3D honeycomb-like micro-patterns formed by both undulated perimysial collagen fibers and different proteins of the ECM. Thus, a scaffold with fibrous structure is crucial for cell organization, survival and function of the seeded cardiac cells. Particularly, nanofibrous electrospun scaffolds have been increasingly investigated for engineering functional cardiac tissue, since they mimic the ECM of native myocardium, they have excellent mechanical properties and fiber properties are easy to manipulate. More importantly, recent advances in electrospun scaffold fabrication with complex structures (e.g., aligned, spring-like fiber) and compositions (e.g., biomolecules, nanoparticles) have made it versatile to endow then with extra properties for facilitating the organization and functionalities of the cardiac tissue. Several studies demonstrated that the presence of aligned surface facilitates the orientation and organization of CMs. For instance, aligned conductive electrospun polyaniline (PANi)/poly (lactic-co-glycolic acid) (PLGA) scaffolds have been demonstrated to promote the organization and coupling of CM in cardiac tissues and their synchronous beating in response to electrical stimulation. Regarding to mechanical properties, several studies demonstrated that a suitable scaffold for cardiac tissue engineering should have

a Young's modulus up to 0.5 MPa and a tensile strength up to 15 kPa, to match the mechanical properties of human myocardium. Moreover, the electrospun scaffold should be biocompatible and its degradation rate should be comparable to the regeneration rate of the native ECM. More than 200 polymers have been investigated to create electrospun scaffold for cardiac tissue engineering, between them only those with excellent biocompatibility have been widely utilized, including both synthetic (e.g. polycaprolactone (PCL), poly-L-lactic acid (PLLA) and polyurethane (PU)) and natural (e.g. gelatin, collagen and silk fibroin) polymers. The results of the literature research revealed that the synthetic polymer of choice for most scientists is PCL. For example, Shin et al. have shown that PCL fiber meshes of 250 nm average fiber diameter suspended on a wire ring support attachment and contraction of neonatal rat CMs in vitro (Figure 12).CMs adhered, populated the entire scaffold mesh, and stained positively for cardio-specific proteins. This highly porous non-woven PCL mesh functions as a temporary ECM that enables the cells to adhere, spread, proliferate and establish electrical communications between layers creating synchronized beating [73].

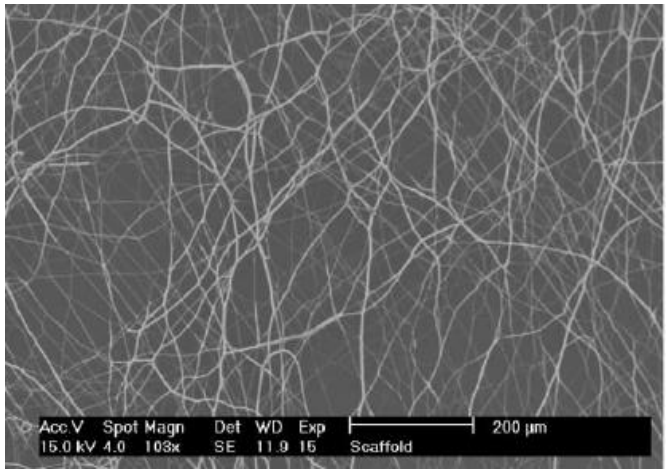

Figure 12. SEM micrograph of mesh.

Nevertheless, the high stiffness and hydrophobicity of the PCL doesn't provide significant cell attachment and proliferation in cardiac tissue engineering. Many studies have been carried out toward the improvement of PCL characteristics. Then combination of PCL with different natural polymers such as collagen, elastin and gelatin has revealed that electrospun PCL/gelatin scaffold showed a higher tensile strength compared to the other hybrid scaffolds [74], [75]. In another study, random and aligned PCL/gelatin composite nanofibrous scaffolds were electrospun to structurally mimic the oriented ECM. Results indicated that PCL/gelatin nanofibrous scaffolds possessed small fiber diameters, increased hydrophilicity and lower stiffness compared to electrospun PCL fibers. The aligned PCL/gelatin nanofibers showed anisotropic wetting characteristic and mechanical properties that closely match the

requirements of native cardiac anisotropy (Figure 13). Rabbit CMs were cultured on electrospun random and aligned nanofibers to asses biocompatibility and potential for cell guidance. It was found out that the aligned PCL/gelatin scaffold greatly promoted cell attachment and alignment because of the biological components and ordered topography of the scaffolds [76].

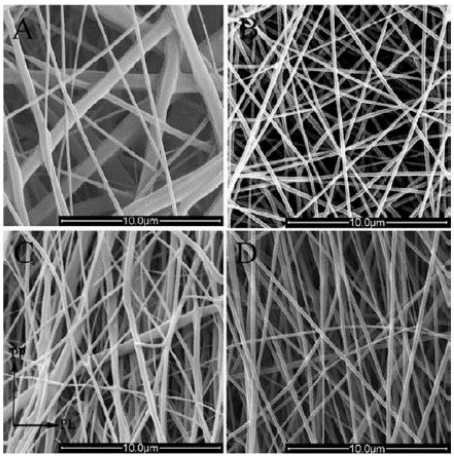

Figure 13. SEM micrographs of electrospun (A) random PCL, (B) random PCL/gelatin, (C) aligned PCL, (D) aligned PCL/gelatin nanofibers.

2. Materials and Methods

2.1 Polycaprolactone

The electrospun scaffolds for the *in vitro* fibrotic cardiac model were fabricated using polycaprolactone (Mw 43000, Polysciences, PCL43). Polycaprolactone (PCL) is a semicrystalline aliphatic polyester produced by ring-opening polymerisation of epsilon-caprolactone (Figure 14). PCL is a biodegradable, biocompatible and nontoxic polymer. It is highly hydrophobic and thus has longer degradation times than polyglycolide (PGA), polylactic acid (PLA), poly(lactic acid-co-glycolic acid) (PLGA) and its copolymers, which makes it suitable for applications where long degradation times are required. PCL is degraded by hydrolysis of its ester linkages in physiological conditions and it has been subject of study for use as an implantable devices. Owing to its low melting temperature (59-64 °C) , PCL is easily processed by conventional melting techniques and can be filled with stiffer materials (particles or fibres) for better mechanical properties. The advantages of PCL for tissue engineering applications include tailorable degradation kinetics and mechanical properties, ease of shaping and manufacture enabling appropriate pore sizes conducive to tissue in-growth and the controlled delivery of drugs contained within their matrix . Functional groups could also be added to make the polymer more hydrophilic, adhesive or biocompatible which enabled favourable cell responses.

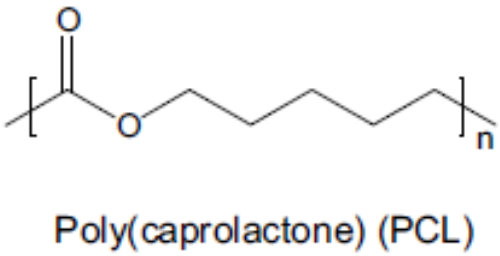

Figure 14. PCL Formula.

2.2 Collagen type I

The collagen subtypes I (Col I) and III (Col III) are essential components of the cardiac extracellular matrix (ECM) maintaining the functional integrity of the heart. In particular, collagen type I accounts for approximately 85% of total myocardial collagens and it is responsible for building thick fibers that endow its tensile strength. Collagen type I is by far the most abundant protein in all vertebrates. It assembles into fibers that form the structural and mechanical scaffold (matrix) of bone, skin, tendons, cornea, blood vessel walls, heart and other connective tissues. It is synthesized as a procollagen precursor, which consists of an N-terminal propeptide, central collagen domain and C-terminal propeptide (Figure 15). The distinguishing feature of all collagens is a triple helix formed by three polypeptide chains with a glycine residue in every third position. The obligatory glycines are essential for the triple-helix formation. Human Collagen type I (Sigma Aldrich-Milano, stored at - 20°C) at 70 µg/mL was used as major component of a biomimetic coating realized on PCL scaffolds to mimic the fibrotic cardiac extracellular matrix. The original product was liquid at a concentration of 1 mg/mL. The Collagen type I solution, at the desired concentration, was solubilized in phosphate saline buffer (PBS) (Life Technologies) under magnetic stirring for 2 h.

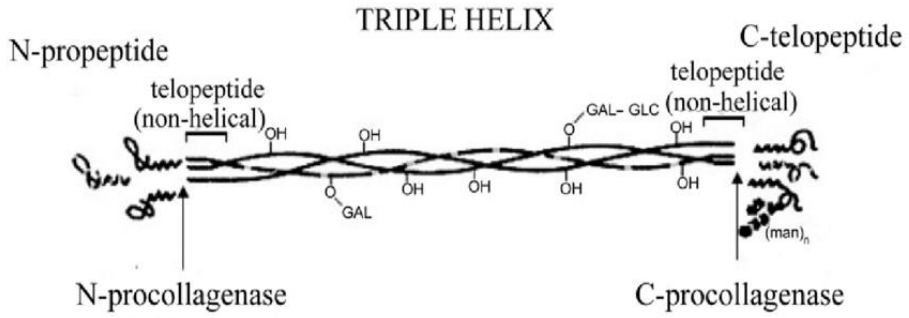

Figure 15. Molecular structure of fibrillar collagen type I.

2.3 Fibronectin

Fibronectin (Fn) is a glycoprotein that provides a scaffold for the infiltration of connective tissue and inflammatory cells. It exists as a protein dimer, consisting of two nearly identical monomers linked by a pair of disulfide bonds (Figure 16). The fibronectin protein is produced from a single gene, but alternative splicing of its pre-mRNA leads to the creation of several isoforms. Fn is expressed in the developing heart and is a minor component of the adult uninjured left ventricle. It is induced in the adult heart in response to MI, produced mainly by fibroblasts and endothelial cells. The alternatively spliced extra domain A (EDA) of fibronectin acts as a pro-inflammatory agent. In addition, fibronectin increases more than 10-fold in the infarcted area at day 2 post-MI and is believed to contribute to an increase in mechanical strength of the infarcted wall.

Fibronectin from human plasma (Sigma Aldrich-Milano, stored at +4 °C) at 30 µg/mL was mixed with collagen type I for biomimetic coating. The fibronectin stock solution was liquid at the concentration of 1 mg/ml. Thus, in order to obtain the desired concentration, the protein solution was solubilized in PBS (Life Technologies) under magnetic stirring for 2 h.

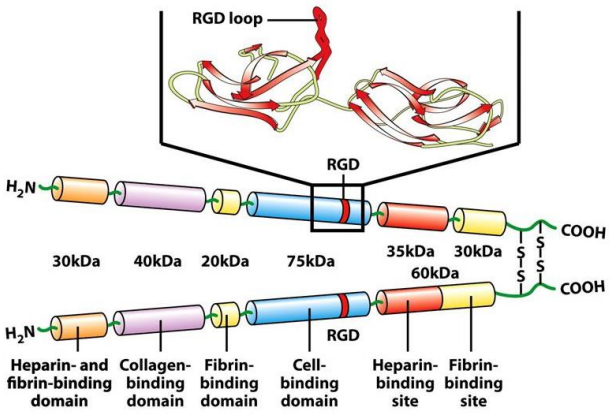

Figure 16. Fibronectin structure.

2.4 Biomimetic coating validation

2.4.1 QCM-D

QCM-D (Biolin, Finland) (Figure 17) was preliminarily used to evaluate the effectiveness of the protein biomimetic coating (polyDOPA/Collagen type I/ Fibronectin) grafting on the adhesive poly-DOPA pre-coating. This analysis allowed to establish the two-step surface functionalization protocol in terms of times and concentrations used.

Figure 17. QCM-D equipement.

QCM-D was used in static configuration and the gold sensor was placed into the chamber. The temperature was set at 20 °C and an initialization procedure was performed. The initialization procedure involved the deposition of 300 µL of Tris/HCl solution on the sensor for 20 min. After this procedure, using a micropipette, DOPA solution (300 µL) was placed on the sensor and left for 7 h, in order to realize the adhesive pre-coating. Finally, the solution was removed and three 5 min washes with Tris/HCl were performed.

2.4.1.1 QCM Collagen type I

After the initialization procedure and the deposition of the adhesive polyDOPA pre-coating on the golden sensor, described above, 300 µL of Collagen type I solution was placed on the sensor, using a micropipette, and left for 16 h. Finally, the solution was removed and three 5 min PBS washes where performed, followed by three 5 min bi-distilled water washes. This

analysis was performed in order to analyse Collagen type I deposition in terms of mass deposited on the sensor and thickness of the protein coating.

2.4.1.2 QCM Fibronectin

Once the initialization procedure and the deposition of the adhesive polyDOPA pre-coating on the golden sensor were performed, an analysis of the deposition of Fibronectin was carried out. The parameters considered were the protein mass deposited on the sensor and the thickness of the coating. In order to perform this analysis, 300 µL of Fibronectin solution were placed on the sensor and left for 16 h. At the end of the 16 h, the solution was removed and the sensor was washed three times for 5 min with PBS and three times for 5 min with bi-distilled water.

2.4.1.3 QCM biomimetic coating

The aim of this analysis is to evaluate the effectiveness of the protein biomimetic coating, taking into consideration the mass of the two proteins deposited on the sensor and the thickness of the mixed proteins coating. After the initialization procedure and the deposition of the adhesive polyDOPA pre-coating on the sensor, as mentioned above, 300 µL of Collagen type I/Fibronectin solution was introduced on the golden sensor and left for 16 h. Then the solution was removed and the sensor was washed three times with PBS (5 min per wash) and three times with bi-distilled water (5 min per wash).

2.4.2 Immunofluorescence staining on golden QCM sensor

Immunofluorescence staining (IF) is a type of immunohistochemistry technique that utilizes antibodies and fluorophores to visualize various cellular antigens such as proteins. This technique can be utilized to visualize the localization of various cellular components within cells, tissues as well as in 3D culture-derived cellular spherical structures. Fluorophores, compounds that emit light when exposed to a certain wavelength of light, are essential for IF. To detect protein expression, the biological sample is incubated with an antibody specific to the protein of interest; the antibody may be coupled to a fluorophore (direct fluorescence) or may be detected by a secondary antibody conjugated to a fluorophore (indirect fluorescence). The proteins or antigens can then be visualized with a fluorescence microscope. Immunostaining on golden QCM sensor, after the deposition of the proteins biomimetic coating, was performed

with the aim of detecting both Fibronectin and Collagen type I deposed on the sensor surface. The procedure was performed following the protocol reported below :

1. cells were fixed in paraformaldehyde (PFA, ThermoFisher Scientific) 4% in PBS for 20 min, followed by 2 washes in PBS. PFA is a cross-linking agent used to preserve and stabilize proteins architecture;
2. samples are blocked with Bovine Serum Albumin (BSA, Sigma Aldrich) 1% in PBS for 30 min. Blocking the sample surface is necessary to avoid non-specific antibody-binding;
3. rabbit anti-Fibronectin primary antibody (Sigma-Aldrich) and Mouse anti-Collagen type I primary antibody (Sigma-Aldrich) were diluted, in BSA (Sigma-Aldrich) 1% in PBS at 1:400 and 1:500 respectively;
4. sensor was incubated with the primary antibodies solution for >1 h at room temperature, follows by 3 washes with PBS, 5 min each;
5. Anti-rabbit secondary antibody, AlexaFluor488 (Life Technologies) and anti-mouse secondary antibody AlexaFluor555 (Life Technologies) were diluted 1:500 in BSA 1%;
6. the sensor was incubated with the secondary antibodies solution for 1 h at room temperature keeping the sensor in the dark to avoid fluorescence bleaching;
7. the sensor was washed 3 times for 5 min with PBS to remove secondary antibody excess and stored at +4°C in PBS solution upon microscope visualization.

The sensor was visualized and imaged with a fluorescence microscope (Nikon Ti2-E) equipped with a digital camera (Nikon Instrument).

2.5 Electrospinning

2.5.1 Optimization of the electrospinning process

The polymeric solution was obtained dissolving polycaprolactone (PCL) in Chloroform/Formic Acid (Sigma Aldrich-Milano) in order to obtain a solution with a final concentration of 20% w/v. The choice of the solvents was made in order to obtain electrospun fibers without defects: Chloroform was chosen because it is very volatile and thus it has a very fast evaporation rate and Formic Acid (reagent ACS > 96%) is required to improve the conductivity of polymeric solution with the aim of increasing the spinnability of PCL, to obtain fibers with a smaller average diameter. The addition of Formic Acid is subsequent, first the PCL is dissolved in Chloroform (70 % v/v) for 4 hours under magnetic stirring and then Formic Acid (30% v/v) is

added. Lastly, the solution is mixed at magnetic stirrer for 40 minutes at 200 rpm to facilitate Formic Acid dispersion. The electrospinning setting is vertical and the device used is the Nova Spider v5 electrospinning tool (Figure 18). The electrospinning device has several components:

i. The high voltage power supply that allows to set a potential difference between 0 kV and 30 kV;
ii. The high-precision volumetric pump that allows to extrude the solution applying a continuous pressure on the syringe;
iii. The 5ml syringe with a 0.8 mm needle, that contains the polymeric solution.
iv. The 190x190 mm flat collector, covered with an aluminium sheet for the deposition of random nanofibers;
v. The 250 mm long x 70 mm of diameter and 4000 rpm drum collector, covered with an aluminium sheet for the deposition of aligned nanofibers;
vi. The movement specification module with an axial velocity of 200 mm/s and an accuracy of 12.5 µm;
vii. The atmosphere controller that allows to set a temperature between 15 and 50 °C and a humidity between 20-80% HR;
viii. The touch screen interface to set the parameters and move the needle.

Figure 18. Nova spider v5 electrospinning tool.

2.5.1.1 Random nanofibers

For the optimization of random nanofibers obtainment, flat collector was used. The electrospinning module was assembled, the syringe containing the polymeric solution was arranged inside the pump, the tube was connected between the syringe and the needle, the positive output of the high voltage generator was interposed between the two and once the whole complex is placed inside the module, the cover is placed with three screws. The optimization step is focused on the optimization of voltage, flow rate and distance between the needle and the collector. Six different sets of parameter where tested (Table 2) to find the combination that allows the obtainment of electrospun nanofibers with small diameter and without defects. The optimization process focused only on the process parameters, as the solution parameters were identified in a previous protocol.

Table 2. Parameters for the optimization of electrospun random nanofiber fabrication protocol.

set	Process parameters
1	Voltage: 15 kV
	Distance: 12 cm
	Flow rate: 0,25 mL/h
2	Voltage: 16 kV
	Distance: 13 cm
	Flow rate: 0,50 mL/h
3	Voltage: 15 kV
	Distance: 12 cm
	Flow rate: 0,50 mL/h
4	Voltage: 15 kV
	Distance: 13 cm
	Flow rate: 0,25 mL/h
5	Voltage: 16 kV
	Distance: 12 cm
	Flow rate: 0,25 mL/h
6	Voltage: 15 kV
	Distance: 13 cm
	Flow rate: 0,50 mL/h

2.5.1.2 Aligned nanofibers

For the optimization of the protocol for the fabrication of aligned nanofibers, rotating drum collector was used. The electrospinning module was assembled as described above. The optimization step is focused on the optimization of voltage, flow rate , distance between needle and collector and collector speed (rpm). Two different sets of parameter where tested (Table 3) in order to choose the protocol that would allow the obtainment of electrospun aligned nanofibers with small diameter and without defects. The optimization process focused only on the process parameters, as the solution parameters were identified in a previous protocol.

Table 3. Parameters for the optimization of electrospun aligned nanofiber fabrication protocol.

set	Process parameters
1	Voltage: 15 kV
	Distance: 12 cm
	Flow rate: 0,25 mL/h
	Collector speed : 2500 rpm
2	Voltage: 15 kV
	Distance: 12 cm
	Flow rate: 0,50 mL/h
	Distance: 12 cm
	Collector speed: 3000 rpm

2.5.2 Membranes fabrication

Once an optimized protocol was established, random PCL electrospun membranes were fabricated setting the process parameters shown in Table 4. The produced membranes were used as scaffold for the cultivation of Cardiac Fibroblasts.

Table 4. Parameters set for PCL membranes fabrication

Process parameters
Voltage: 16 kV
Flow rate: 0.5 mL/h
Distance: 13 cm

The flat collector was covered with an aluminium foil in order to make the surface conductive. Once the foil was fully covered, the membranes were detached from the aluminium foil and mounted on coverslips.

2.6 Surface modification by polyDOPA and Collagen type I/Fibronectin

The electrospun membranes surface was functionalized through biomolecules in order to make the scaffold surface biomimetic. In particular the protocol involves a two-step surface modification process. Fist an adhesive polyDOPA pre-coating and then a biomimetic Collagen type I/Fibronectin coating.

To realize the adhesive coating, a slightly basic solution was prepared to induce the self-polymerization of 3,4- Dihydroxy-DL-phenylalanine (DOPA). Inspired by mussel-adhesion phenomena in nature, Dopamine, a biomolecule which contains catechol and amine functional groups, can mimic the powerful adhesion exerted by mussels. Generally, under week alkaline aqueous conditions and in the presence of oxygen at room temperature, dopamine can self-polymerize into polydopamine (pDA) (Figure 19), which spontaneously deposits a thin adherent coating onto various material surfaces. More importantly, these formed adherent polydopamine coatings have a surface containing ample active catechol and amine groups, able to serve as reductants, binding reagents and universal platforms for the secondary reactions.

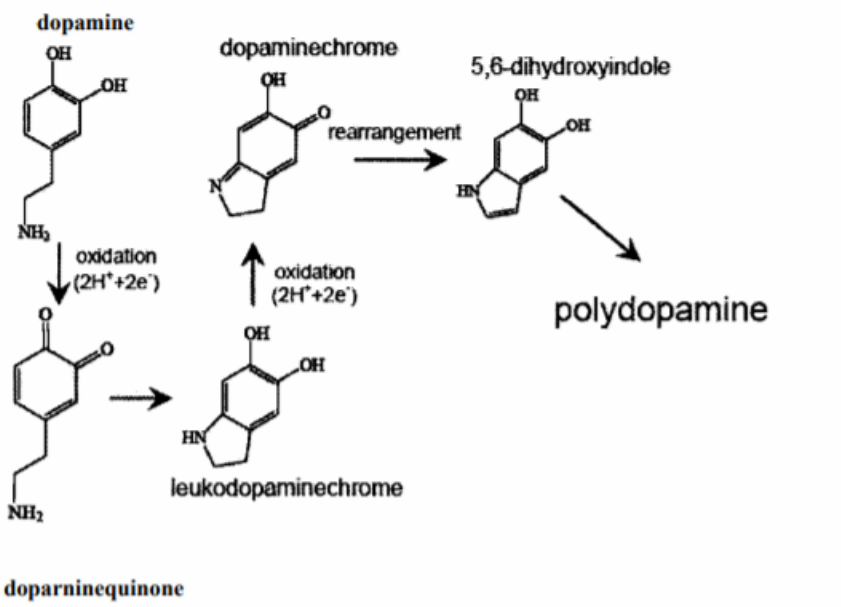

Figure 19. Mechanism for polydopamine formation.

The basic buffer needed to induce the DOPA self-polymerization was produced dissolving tris(hydroxymethyl)aminomethane (ACS reagent, >=99.8%) 10 mM in double distilled water. After that, HCl (1M) was added in order to obtain a solution with pH equal to 8.5 (Tris/HCl solution). The DOPA (Sigma-Aldrich, 2 mg/mL) was solubilized in the Tris/HCl solution (pH 8.5). To obtain the adhesive pre-coating, PCL membranes were dipped into the DOPA solution, once the polymerization had begun, which is when the solution had begun to turn brown. The membranes were left in immersion at room temperature for 7 hours. These parameters have been optimized by a previous protocol. After the 7 hours functionalization, the membranes were removed from the solution and 3 washes of 5 minutes in Tris/HCl solution were made to remove the polyDOPA excess not bonded to the surface [77] .

The biomimetic coating was obtained mixing human Collagen type I and Fibronectin, with a percentage of 70% and 30% respectively. The two protein solution where dissolved in PBS (Life Technologies) under magnetic stirring for 2 hours. Finally, the PCL/DOPA electrospun membranes were dipped in the proteins solution in static conditions at room temperature for 16 hours. Then, they were washed three times, for 5 minutes in PBS and finally a bi-distilled water final wash was performed.

2.7 PCL-based Scaffold characterization

2.7.1 Scanning Electron Microscope (SEM)

The PCL electrospun scaffolds were morphologically characterized using an electronic scanning microscope (SEM) (ZEISS Supra 40 Field Emission Scanning Electron Microscopy) (Figure 20). In order to perform this analysis, the samples were first coated with a thin gold layer and then inserted in the SEM chamber.

Figure 20. ZEISS Supra 40 Field Emission Scanning Electron Microscopy.

Images were obtained at different magnifications (1000x, 2000x, 5000x, 10000x, 20000x, 50000x) using a lens-sample distance of 10.3 mm and a beam voltage of 10 kV. The SEM analysis was performed at the DISAT department of the Turin Polytechnic.

2.7.2 ImageJ Software

ImageJ digital image processing software (National Institute of Health, USA) was used to process SEM images of the produced electrospun membranes, in order to determine the distribution of fiber diameters and the porosity of the membranes. To determine the average diameter, the proper dimensional scale was set and 100 diameters were measured from an image with high magnification (5000X). Porosities were qualitatively determined from a SEM image at high magnification (5000X). The threshold parameters, both the lower and upper limits, were arbitrarily based on membrane morphology. The obtained data were processed with Excel software in order to calculate the average diameter, the average porosity in terms of area

(μm^2) and theirs relative standard deviations. Subsequently the distribution graphs were obtained processing the results with GraphPad Prism 9.1.1 software.

2.8 Surface modification characterization

2.8.1 Immunofluorescence staining

Immunofluorescence staining was performed on the functionalized PCL-based scaffold in order to analyse the biomimetic coating surface morphology and to visualize the distribution of Collagen type I and Fibronectin on the scaffold surface. The protocol used was the same of the immunofluorescence staining performed on the golden QCM sensor (Steps 1-7). Finally, sample was visualized and imaged with a fluorescence microscope (Nikon Ti2-E) equipped with a digital camera. (Nikon Instrument).

2.8.2 BCA protein assay kit

The BCA Protein Assay Kit (Thermo Scientific Pierce) provides a colorimetric method for detection and quantification of proteins. This method combines the reduction of Cu^{+2} to Cu^{+1} by protein in an alkaline medium with the sensitive detection of the cuprous cation (Cu^{+1}) using a unique reagent containing bicinchoninic acid (BCA). The presence of proteins causes a change in the colour of the solution, from green to purple. The purple-coloured reaction product is formed by the chelation of two molecules of BCA with one cuprous ion. The obtained water-soluble product has a strong absorbance at 562 nm that is approximately linear as the protein concentration increases over a range between 20 and 2000 µg/ml. Mostly, protein concentrations are determined and reported with reference to standards of bovine serum albumin (BSA). Diluted albumin standards were prepared based on the working concentration range. Working Reagent was prepared mixing 50 parts of BCA reagent A with 1 part of BCA reagent B (50:1, Reagent A:B). 50 µL of each standard were mixed into a 24-multiwell plate with 400 µL of Working Reagent in order to obtain the calibration curve. Samples were placed in the multiwell plate and treated with 50 µL of diluent (PBS) and 400 µL of Working Reagent. Plate was then incubated for 30 min at 37 °C and subsequently 100 µL were moved from each well and placed in a 96-multiwell plate. Finally the absorbance was measured at 562 nm on a plate reader (Synergy HTX Multi-Mode Microplate Reader, BioTek).

2.8.3 Coating stability test

Coating stability at 7 days was assessed incubating the polyDOPA/Collagen type I/Fibronectin functionalized PCL scaffold in physiological media (Fibroblasts Growth Medium-3, PromoCell). After 24 hours and 7 days, BCA protein kit assay was performed on the samples, in order to evaluate the quantity of proteins grafted on the surface, using the protocol reported above.

2.9 Cell culture maintenance and analyses

2.9.1 Human Cardiac Fibroblasts culture expansion

The cell source chosen for the bidimensional *in vitro* model of cardiac fibrosis was Human Cardiac Fibroblasts (HCF) isolated from the ventricles of adult heart (PromoCell) (21). HCF were maintained in Fibroblasts Growth Medium-3 (PromoCell), containing Basal medium with the supplement of 10% Fetal Calf Serum, 1 ng/mL Basic Fibroblast Growth Factor (recombinant human) and 5 µg/ml Insulin (recombinant human).

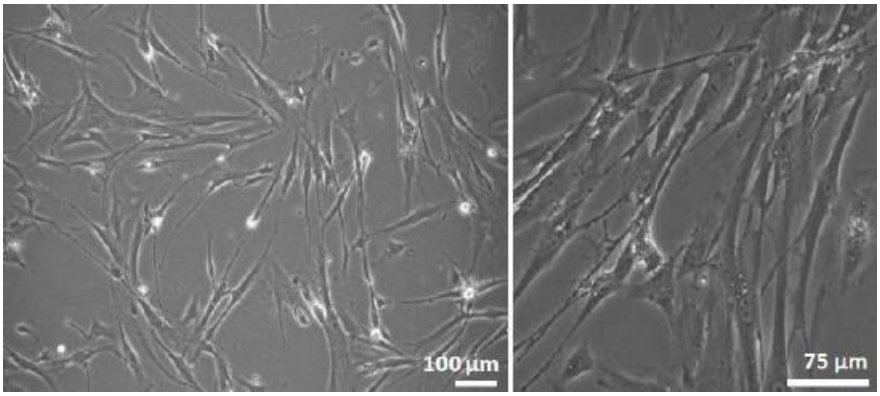

Figure 21. Human Cardiac Fibroblasts used in biological tests.

During culture, they are maintained in an incubator at 37 °C and 5% CO_2. In order to maintain cells healthy and allow them to proliferate, it is necessary to split them in a new plate during the culture period and to periodically replace the culture medium with fresh medium. Cell passage in a new plate is called trypsinization, consisting in cell dissociation using trypsin. Trypsin is a proteolytic enzyme which promotes membrane glycoprotein lysis responsible for cell adhesion, allowing to dissociate adherent cells from the dish in which they are being cultured. When the trypsinization process is complete, cells will be appear suspended and

rounded. This process is necessary in a confluent culture in order to avoid contact inhibition and accumulation of toxic product as results of a slowing down of cell metabolism.

Trypsinization protocols involves several steps:

1. evaluation of cell confluence through optical microscope (Leica Microsystems);
2. removal of the culture medium, since fetal calf serum inhibits trypsin action;
3. wash with 3 ml of PBS to remove dead cells, cells debris and medium residues;
4. PBS removal;
5. addition of a volume of Trypsin/EDTA (Life Technologies) based on the size of the culture dish;
6. incubation at 37 °C for 3 min;
7. evaluation of the effectiveness of the treatment in terms of cell detachment under the microscope;
8. trypsin inactivation by adding a double volume of fresh medium;
9. collect the cell suspension into a 15 mL tube;
10. wash the plate with 3-4 mL of PBS;
11. collection of PBS in the cell tube;
12. centrifugation at 300g for 5 min to pellet cells;
13. removal of the supernatant;
14. re-suspension of the pellet in fresh medium.

After this process, cells may be counted using the NEUBAUER improved counting chamber (Figure 22). When the chamber is observed under the optical microscope, the countering grid is composed of 9 big squares (1x1 mm). Among them, the four squares at the corners, delimited by triple lines, contain 16 medium sized squares each measuring 0.05 x 0.05 mm. The cells confined in the 4 corner squares plus those on two contiguous sides of each square are counted. 40 µl of cell suspension were taken and loaded below the chamber cover glass and the grid is observed under the microscope. The total number of cells can be obtained with the following formula:

- n. cells TOT = $\left(\frac{A+B+C+D}{4}\right) \cdot 10^4 \cdot V$

Where A,B,C and D represent the four squares taken into consideration and V the final volume of the suspension. Once the total number of cells is obtained it is possible to seed them in

variable number of culture dishes, depending on the desired number for the planned experiments.

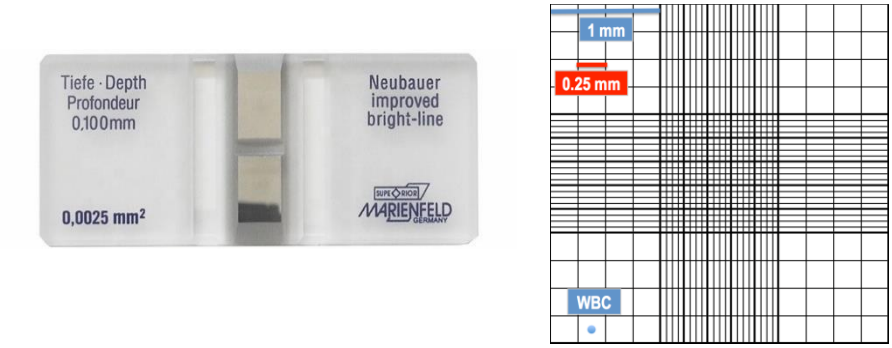

Figure 22. NEUBAUER cell counting chamber and grid.

2.9.2 PCL electrospun membranes processing and cell seeding

Glass slides coated with PCL membranes with polyDOPA/Collagen type I/Fibronectin grafting and glass slides coated with Gelatin as control were placed into a 24-multiwell. The slides with PCL membranes were previously disinfected by immersion in 70% v/v ethanol (EtOH) for 15 min, followed by rinsing in sterile PBS. Then membranes were exposed to UV irradiation for 30 min on each side and incubated overnight in 2X antibiotic-antimycotic solution (Life Technologies) in PBS, followed by PBS rinsing, to decrease bacterial contamination risk. Each sample was seeded with 25000 cells in a volume of 30 µL. PBS was added in the empty volume between wells before placing the plate in the incubator, in order to minimize medium evaporation during cell attachment. After 1 h, 500 µL of medium were added in each well. Culture medium is replaced with fresh medium every 2-3 days in order to keep cell culture in optimal condition. Cells were analysed for viability and cytotoxicity with Cell Titer Blue Cell Viability assay (Promega) and CytoTox-ONE™ Homogeneous Membrane Integrity Assay (Promega), respectively, after day 1 and 7 of culture. In addition Phalloidin/DAPI staining was performed to evaluate cell morphology and cytoskeletal organization.

2.9.3 Cell Titer Blue Cell Viability Assay

The CellTiter-Blue Cell Viability Assay is used as a fluorometric method to evaluate the viability of cell and to estimate the number of viable cells on the PCL membranes coated with polyDOPA/Collagen type I/Fibronectin. The Reagent (Promega) contains highly purified resazurin, that is used as an indicator: in an oxidated environment resazurin is blue and it turns

purple in reduced environment. Viable cells are metabolically active and they are able to reduce resazurin into resorufin, that is highly fluorescent, while nonviable cells lose metabolic capacity, they can't reduce resazurin and thus there is no fluorescent signal generation (Figure 23).

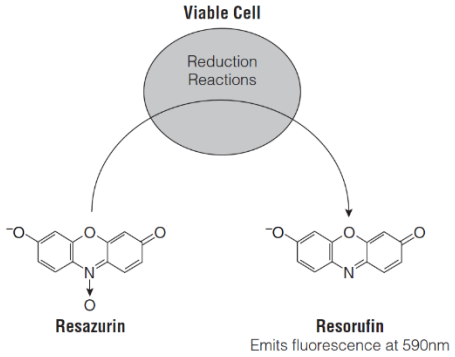

Figure 23. Reduction of resazurin to resorufin by viable cells.

The CellTiter reagent is diluted 1:10 in Fibroblasts Growth Medium-3 (PromoCell). Each sample is placed into a multiwell plate and it is treated with 500 µL of solution and placed in incubator for 4 h. 100 µL are taken from each well and placed into a 96-well. The fluorescent emission of Resorufin is at 590 nm and it results from an excitation at 530 nm. The signal is read using a plate reader (Synergy HTX Multi-Mode Microplate Reader, BioTek) and its intensity is directly proportional to the number of viable cells.

2.9.4 CytoTox-ONE^{TM} Homogeneous Membrane Integrity Assay

Cytotoxicity is evaluated by CytoTox-ONE^{TM} Homogeneous Membrane Integrity Assay, that provides a homogeneous, fluorometric method to estimate the number of non-viable cells on the protein coated scaffold and on the control. Cell viability can be defined based on the integrity of the cell membrane and can be measured observing the exclusion of vital dyes. CytoTOX-ONE assay is a 10 min coupled enzymatic assay consisting in the measure of the release of lactate dehydrogenase (LHD) in the medium from cells with damaged membrane. The measure is based into the conversion of resazurin into resorufin, the generation of fluorescent resorufin product is proportional to the amount of LHD (Figure 24).

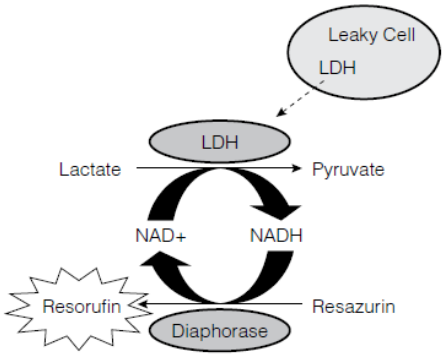

Figure 24. Release of LDH from damaged cells.

The product is supplied as a lyophilized Substrate Mix and it is reconstituted with assay buffer to obtain the CytoTOX-ONE reagent. The medium is taken from the multiwell plate and placed into a new one. Lysed cells are used as control. 100 µL of CytoTOX-ONE reagent is added to each well and incubated for 10 minutes. Then 50 µL of Stop Solution is added and the content of each well is moved into a 96-well. The fluorescent signal is measured using a plate reader (Synergy HTX Multi-Mode Microplate Reader, BioTek), using 530 nm as excitation wavelength and 590 nm as emission wavelength. The intensity of fluorescence produced is proportional to the number of lysed cells.

2.9.5 Phalloidin Staining

Phalloidin is a selective bicyclic peptide that is used for staining actin filaments (F-actin) as it binds to all variant of actin filaments in many different species of animals. Typically, it is used conjugated to a fluorescent dye, such as Rhodamine. Phalloidin is used on fixed samples, using PFA as fixative. In order to perform the staining, cells were seeded on PCL scaffold, PCL scaffold functionalized with polyDOPA and Collagen type I/Fibronectin and on coverslips coated with Gelatin and subsequently fixed at day 1, 3 and 7 of culture. The protocol used is reported below:

1. cell fixing in paraformaldehyde (PFA, ThermoFisher Scientific) 4% in PBS, for 20 min, followed by 3 washes in PBS;
2. cells permeabilization with Triton X-100 (Sigma-Aldrich) 0.5 % in PBS for 8 min, followed by 2 washes in PBS. Triton X-100 is used to increase cells permeability to favour antibodies penetration;

3. samples incubation with Phalloidin-Rhodamine and DAPI, both diluted 1:1000 in BSA 1%, for 45 min at room temperature, followed by 3 washes in PBS;
4. samples storing in PBS at +4°C, upon microscope analysis.

3. Results

This section shows all the results concerning the optimization and fabrication of PCL-based electrospun membranes. In addition, as a protein biomimetic coating has been grafted on the PCL membranes surface, the results about the validation and the characterization, confirming the functionalization, are also presented. In conclusion, all the results concerning the HCF cultures carried out on the functionalized scaffold, as biological validation, are reported.

3.1 Biomimetic coating validation

3.1.1 QCM-D

3.2.1.1 QCM-D Collagen type I

The quartz crystal microbalance with dissipation monitoring (QCM-D) allowed the recording of mass deposition. The two-steps deposition of polyDOPA/Collagen type I was monitored real time in order to quantify the amount of grafted Collagen type I on polyDOPA adhesive pre-coating.

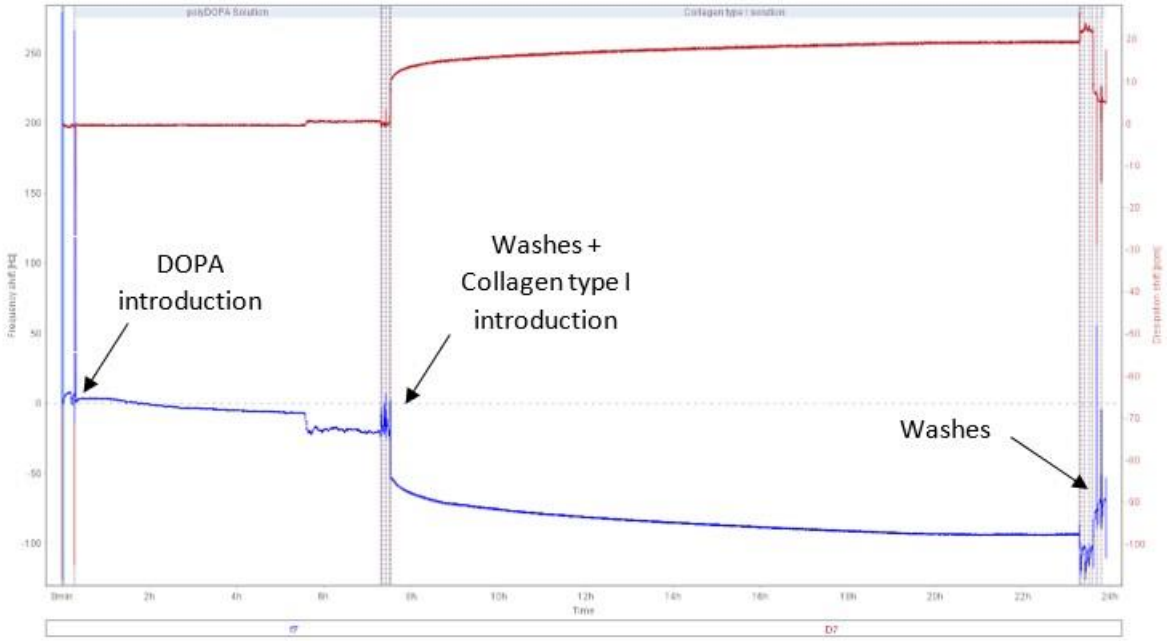

Figure 25. QCM-D of polyDOPA/Collagen type I deposition. Blue and red curves represent the frequency shift and the dissipation, respectively.

Figure 25 shows frequency shift and dissipation curves for polyDOPA and Collagen type I deposition. Considering the entire acquisition, it can be seen a decrease of frequency shift from 0 to about -120 Hz. This result demonstrates the successful mass deposition on the crystal. During the first 7 h, corresponding to polyDOPA functionalization step, the frequency shift decreases until -30 Hz , demonstrating the effective polyDOPA deposition. At the end of the 7 h, polyDOPA solution was removed, the sensor was washed and Collagen type I solution was added by a micropipette. In correspondence of the washes, both frequency shift and dissipation curves show a noisy signal. When the Collagen type I is added there is a sudden drop in frequency shift and a corresponding increase of dissipation: such trend continues until the end of the acquisition. This result demonstrates Collagen type I deposition. Dissipation is related to the substrate mechanical properties and as polyDOPA is a rigid substrate, dissipation increase is negligible, while during Collagen type I deposition the increase is marked, as Collagen type I is a soft substate. Moreover, it is possible to observe that the deposition is more marked in the first hours but it stabilizes only at the end of the 16 h, therefore in defining the functionalization protocol timing for the future functionalization of the scaffolds, the scaffolds will be dipped for 16 h in the Collagen type I solution. At the end of the acquisition, mass and thickness of the two layers deposited on the sensor were calculated in order to evaluate the effectiveness of Collagen type I grafting on polyDOPA (Figure 26 and Figure 27).

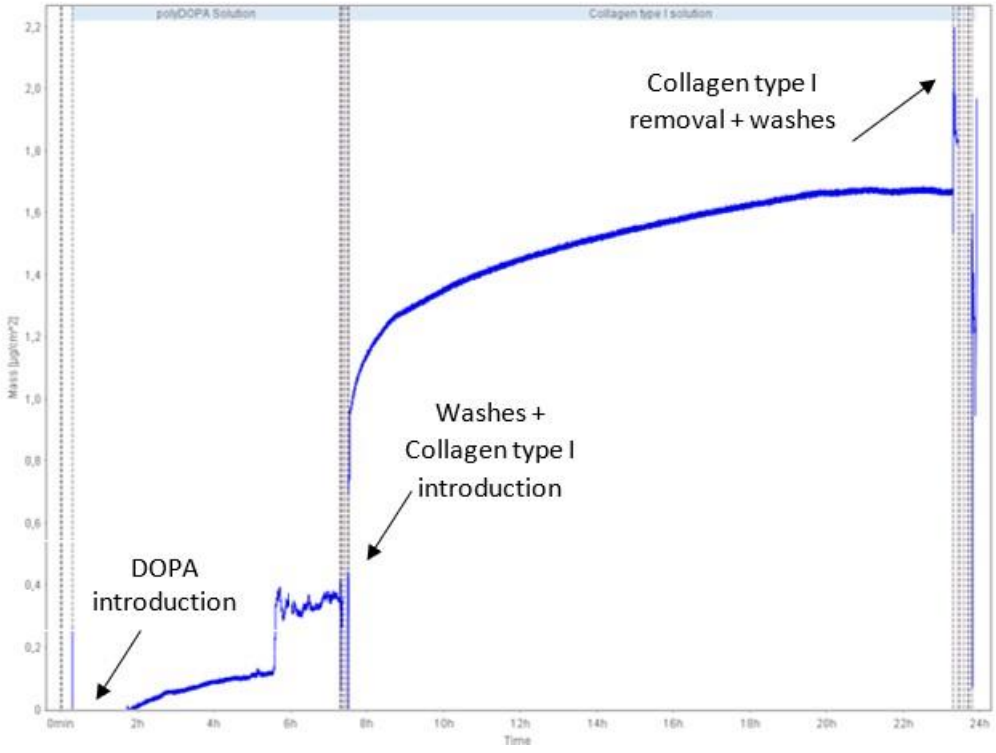

Figure 26. Deposited Collagen type I mass analysis.

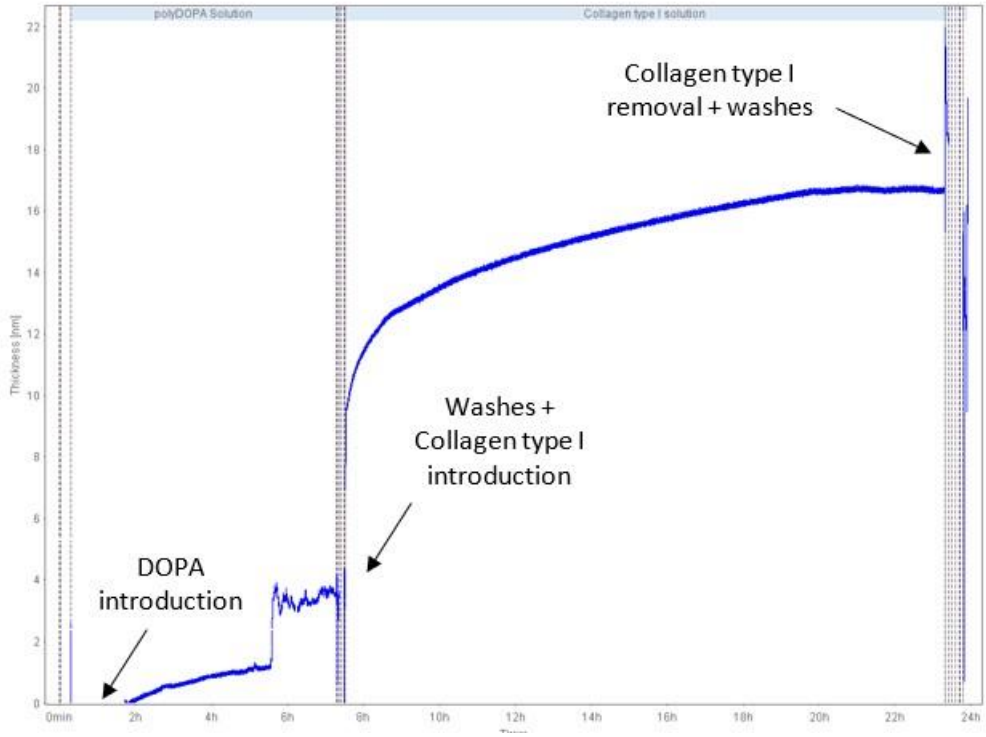

Figure 27. Thickness of the deposited Collagen type I layer analysis.

Figure 26 shows the trend over time of the mass deposited on the sensor. During the polyDOPA deposition the mass increased from 0 to 0.4 µg /cm^2 and at the end of the acquisition the mass deposited on the sensor was 1.6 µg/cm^2. These results suggest the successful grafting of Collagen type I. Considering the surface area of the golden sensor (1.54 cm^2), at the end of the acquisition the mass on the sensor was 2.47 µg. The quantity of polyDOPA deposited was 0.61 µg, thus subtracting this quantity to the total mass on the sensor, it is possible to obtain the mass of Collagen type I deposited, that was 1.86 µg. In conclusion, the mass ratio of deposited Collagen type I to polyDOPA was around 3:1 (wt/wt).

Figure 27 allows to calculate the thickness of the Collagen type I coating on the sensor. The thickness of the adhesive polyDOPA pre-coating was 4 nm and at the end of the acquisition the thickness of the adlayer on the sensor was 16 nm. This results indicates the deposition of a 12 nm thick Collagen type I coating .

3.2.1.2 QCM-D Fibronectin

The deposition of the adhesive polyDOPA pre-coating and the subsequent deposition of Fibronectin were analysed though QCM-D. The aim of the analysis was monitoring the two-step functionalization and calculating the mass deposited on the golden sensor and the thickness of the adlayer.

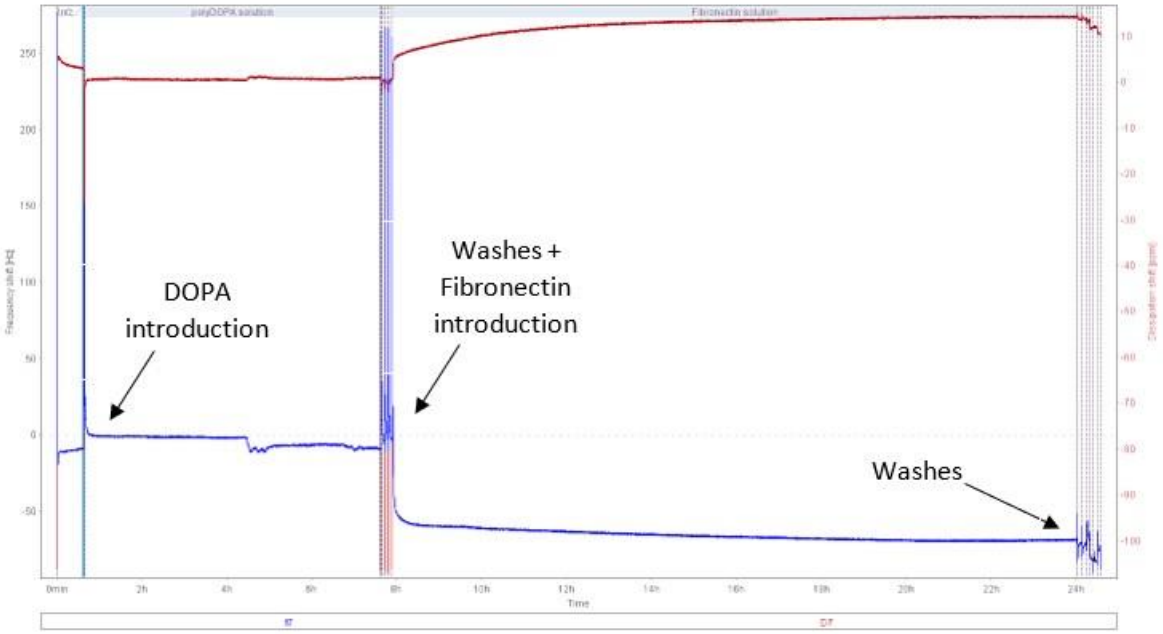

Figure 28. QCM-D of polyDOPA/Fibronectin deposition. Blue and red curves represent the frequency shift and the dissipation, respectively.

The frequency shift and dissipation curves are shown in Figure 28. During all the acquisition the frequency shift decreased from 0 to about -90 Hz, demonstrating successful mass deposition on the QCM-D sensor. The deposition of polyDOPA was demonstrated by a frequency shift value of -10 Hz after 7 h. Then, the polyDOPA solution was removed, the sensor was washed and Fibronectin solution was added. Washing steps were characterized by a noisy signal both on frequency shift and dissipation curves. During the addition of Fibronectin solution and during the following 16 h, the frequency shift suddenly decreased and dissipation increased, as a proof of Fibronectin grafting on the polyDOPA layer. After the real-time acquisition, mass and thickness of the adlayer were calculated (Figure 29 and Figure 30).

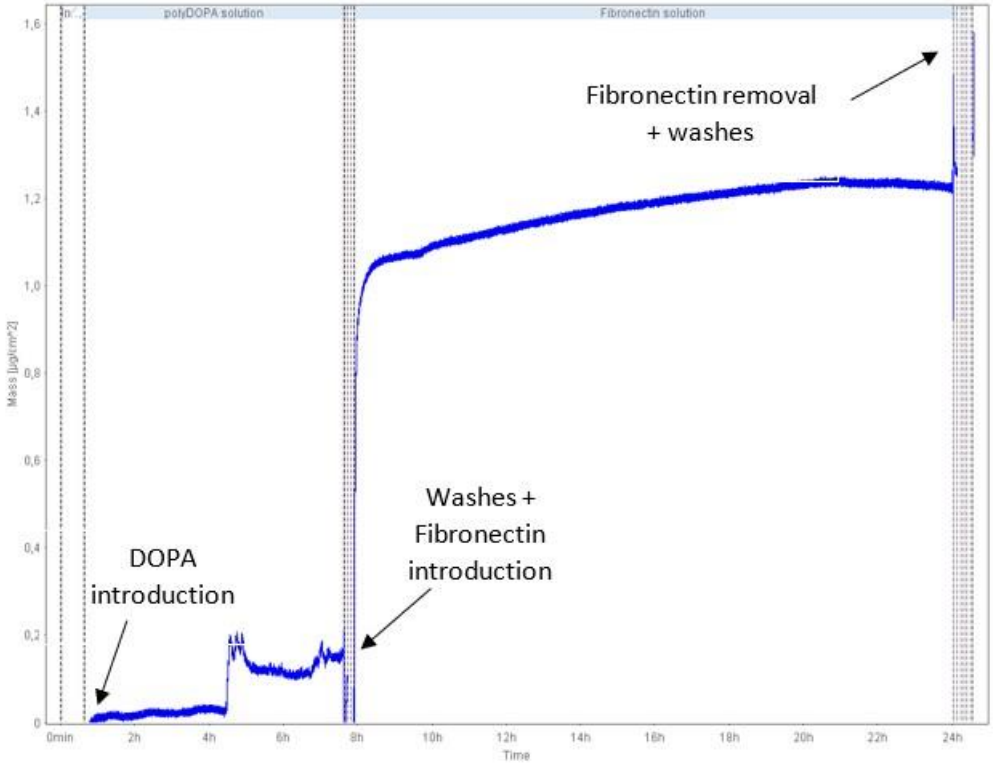

Figure 29. Deposited Fibronectin mass analysis.

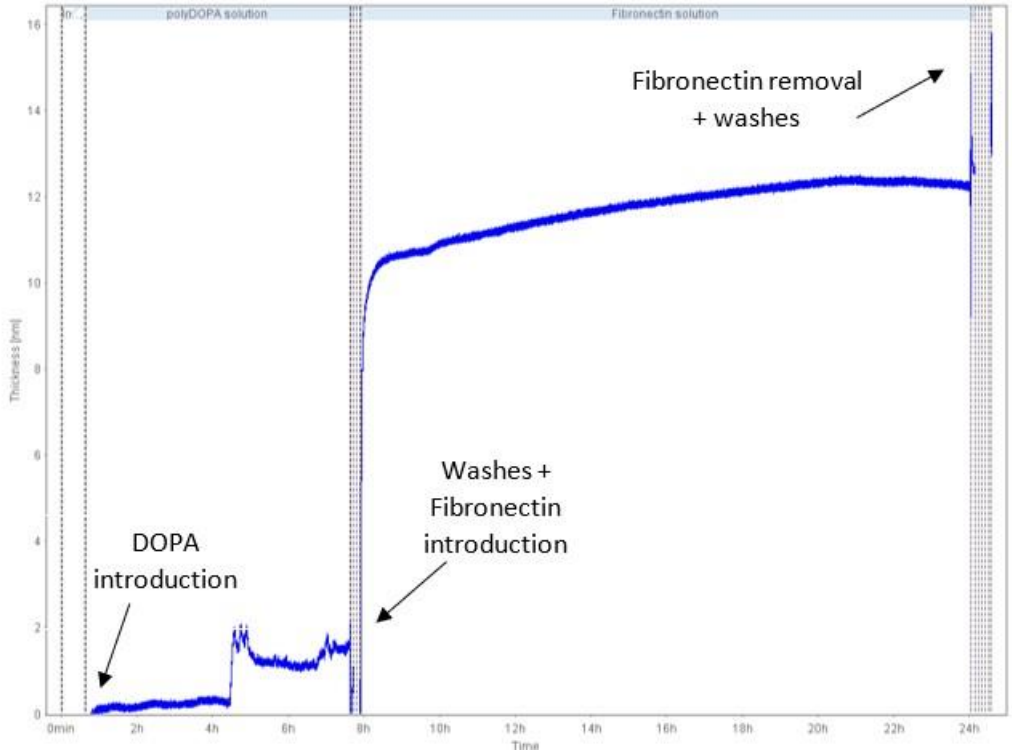

Figure 30. Thickness of the deposited Fibronectin layer analysis.

Figure 29 refers to the trend of the mass deposited on the sensor. After the polyDOPA deposition, the mass on the sensor was 0.17 µg /cm^2 and at the end of the acquisition it was 1.30 µg/cm^2 . Considering the golden sensor surface area (1.54 cm^2), it was possible to calculate both the polyDOPA mass and the Fibronectin mass deposited on the sensor. The quantity of polyDOPA deposited was 0.27 µg and at the end of the acquisition the deposited mass was 2,002 µg. Then subtracting the mass of polyDOPA from the total mass on the sensor it was possible to obtain the mass of grafted Fibronectin, which was 1.732 µg. In conclusion, the mass ratio of deposited Fibronectin to polyDOPA was around 6.4:1 (wt/wt).

Figure 30 allowed to calculate the thickness of Fibronectin coating on the sensor. Considering all the acquisition, the thickness of the adlayer increased from 0 to 13.03 nm, consisting of 1.6 nm thick polyDOPA pre-coating and 11.43 nm thick Fibronectin coating.

3.2.1.3 QCM-D biomimetic coating

The successful Collagen I/Fibronectin biomimetic protein coating on the adhesive polyDOPA pre-coating was also assessed by QCM-D analysis.

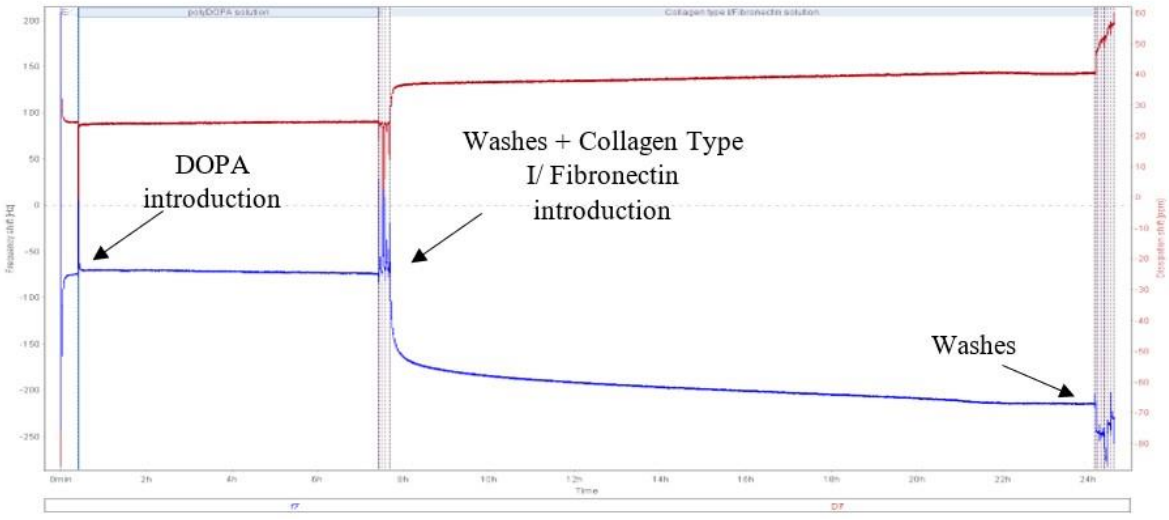

Figure 31. QCM-D of polyDOPA/Collagen type I / Fibronectin deposition. Blue and red curves represent the frequency shift and the dissipation, respectively.

Frequency shift and dissipation were monitored in real time (Figure 31). Mass deposition on the QCM-D sensor was detected at the end of the analysis, supported by a decrease in frequency

shift from 0 to about -296 Hz during the entire acquisition. The deposition of the polyDOPA adhesive pre-coating on the golden sensor was proven by frequency shift of about -100 Hz after 7 h. After, the sensor was washed three times for 5 min with Tris/HCl, to remove the polyDOPA excess and then Collagen type I/Fibronectin solution was added using a micropipette. The noisy signal both in frequency shift and dissipation was due to washes. The addition of the protein solution caused a sudden decrease in frequency shift and an increase in dissipation, maintaining the same trend for the following 16 h. After washing, a further decrease in frequency was observed, due to coating swelling during washes. Therefore, the signal could be due to the absorption of water. This phenomenon was more evident in this case rather than in the single deposition of proteins because there is a reciprocal relationship between Collagen type I and Fibronectin. Indeed, Fibronectin is thought to accelerate the early stages of Collagen assembly and Collagen fibrillogenesis is thought to catalyse the formation of Fibronectin fibrils [78]. These results suggest a successful grafting of the biomimetic protein coating to the polyDOPA pre-coating. In addition, mass and thickness of the adlayer were calculated at the end of the real-time acquisition (Figure 32 and Figure 33).

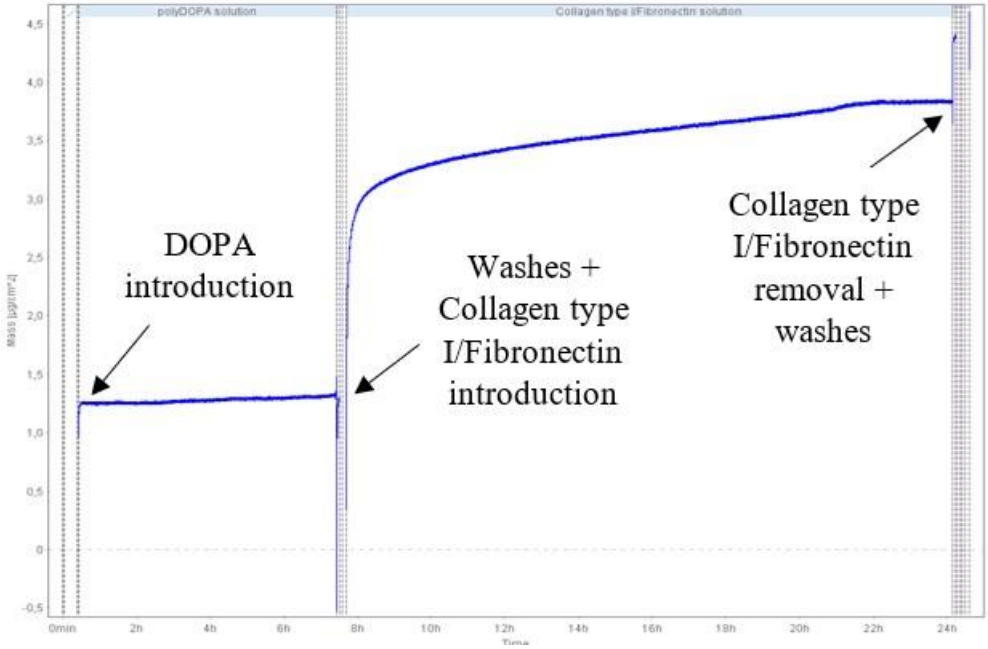

Figure 32. Deposited Collagen type I/ Fibronectin mass analysis.

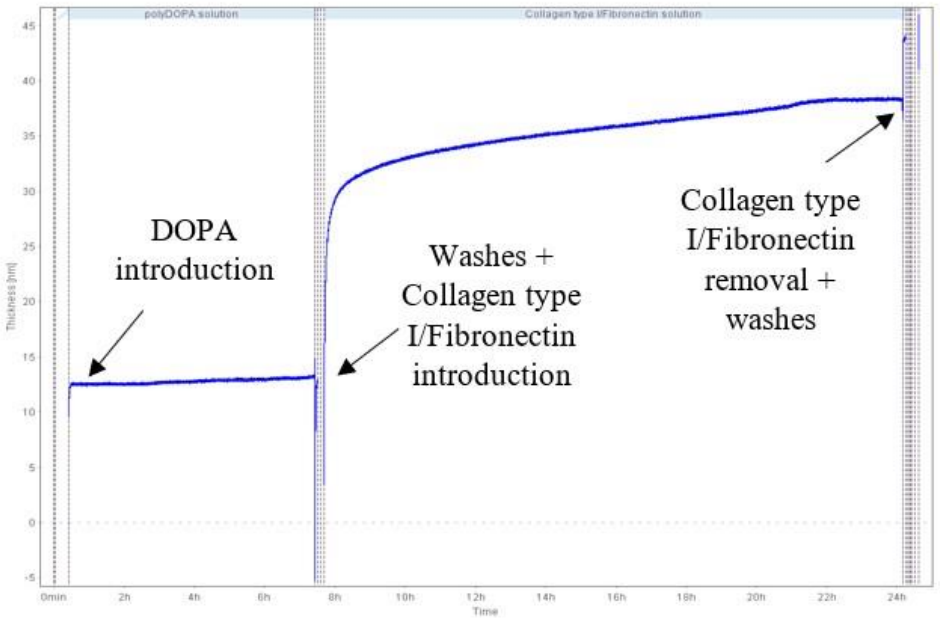

Figure 33. Thickness of the deposited Collagen type I /Fibronectin layer analysis.

The trend of the mass of Collagen type I/Fibronectin on the golden sensor is shown in Figure 32. PolyDOPA deposition was characterized by an increase in mass that took a value of 1.72 µg /cm^2 after 7 hours. At the end of the acquisition the mass deposited on the sensor was 5.30 µg/cm^2 . The increase of mass is an indicator of a successful grafting of the two proteins mix on the polyDOPA layer. Considering the sensor surface area (1.54 cm^2) mass value was calculated. Hence the quantity of polyDOPA deposited was 2.65 µg and the quantity of Collagen type I/Fibronectin was 5.51 µg.

Figure 33 displays the results of the thickness analysis and allowed to calculate both the thickness of the polyDOPA adhesive pre-coating and of the protein biomimetic coating on the sensor. The polyDOPA layer on the sensor was 17.17 nm thick and the grafted protein coating had a thickness of 35.83 nm.

In conclusion, Table 5 reports the characteristics of the grafted protein layers, in terms of mass and thickness, both in the case of single protein deposition and of two protein simultaneous deposition. It is possible to observe that the mass is higher when the two proteins are deposited together with respect to single deposition, this can be due to the Collagen type I and Fibronectin molecular interaction that leads to protein packing and to an ECM-like network assembly [78].

Table 5. Characteristics of grafted Collagen type I, Fibronectin and Collagen type I/Fibronectin layers measured by QCM-D

		Mass (µg)	Thickness (nm)
Collagen type I deposition	polyDOPA	0.61	4
	Collagen type I	1.86	12
Fibronectin deposition	polyDOPA	0.27	1.6
	Fibronectin	1.73	11.43
Collagen type I/Fibronectin deposition	polyDOPA	2.65	17.17
	Collagen type I/Fibronectin	5.51	35.83

3.2.2 Immunofluorescence staining on gold QCM sensor

This analysis was made to confirm Collagen type I and Fibronectin deposition on the golden QCM sensor and thus the deposition of the biomimetic protein coating on the polyDOPA adhesive layer. The detection of the two proteins was made by indirect immunofluorescence: Collagen type I secondary antibody was labelled in red while Fibronectin secondary antibody was labelled in green. Thus, red and green fluorescence corresponded to Collagen type I and Fibronectin, respectively (Figure 34).

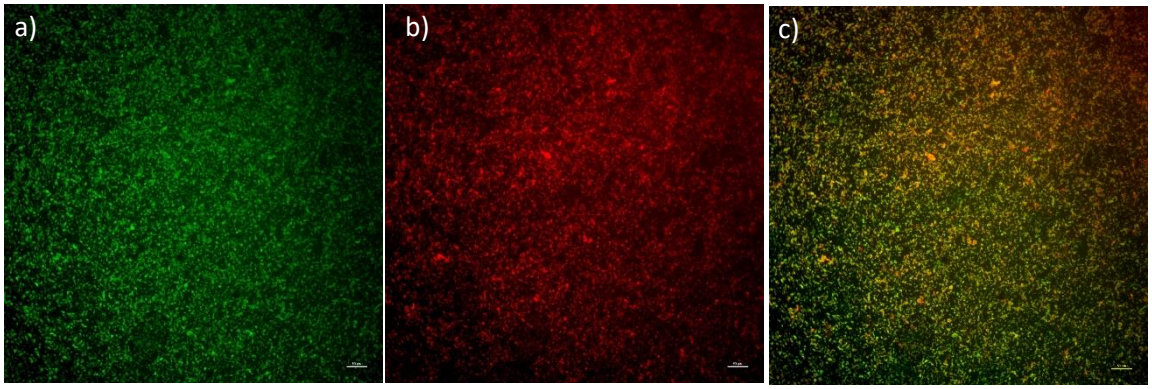

Figure 34. Immunofluorescence staining of golden sensor after the coating: a) Fibronectin (labelled with AlexaFluor488) , b) Collagen type I (labelled with AlexaFluor555), c) merged image. Bar scale 50 µm.

Immunofluorescence images in Figure 34 demonstrated the presence of both Collagen type I and Fibronectin on the adhesive polyDOPA layer on the golden QCM sensor. Distribution of the fluorescence signals suggested uniform spatial distribution of the two proteins on the sensor surface, as a further proof of the successful deposition of the biomimetic coating. Particularly, in some regions of the sensor, the two fluorescence signals were superposed, suggesting the presence of two different overlapping protein layers.

3.2 Electrospun membrane optimization

3.2.1 Scanning Electron Microscope (SEM): morphological analysis

3.2.1.1 Random nanofibers

Scanning Electron Microscopy (SEM) was performed to evaluate the electrospun fibers morphology in order to establish an optimized set of processing parameters. Only the membranes obtained from process with continuous good spinnability were evaluated by SEM analysis. Among the six sets of process parameters investigated for the optimization process, only two were selected (Table 6).

Table 6. Selected process parameters for electrospinning process

set	Process parameters
1	Voltage: 15 kV
	Distance: 12 cm
	Flow rate: 0,25 mL/h
2	Voltage: 16 kV
	Distance: 13 cm
	Flow rate: 0,50 mL/h

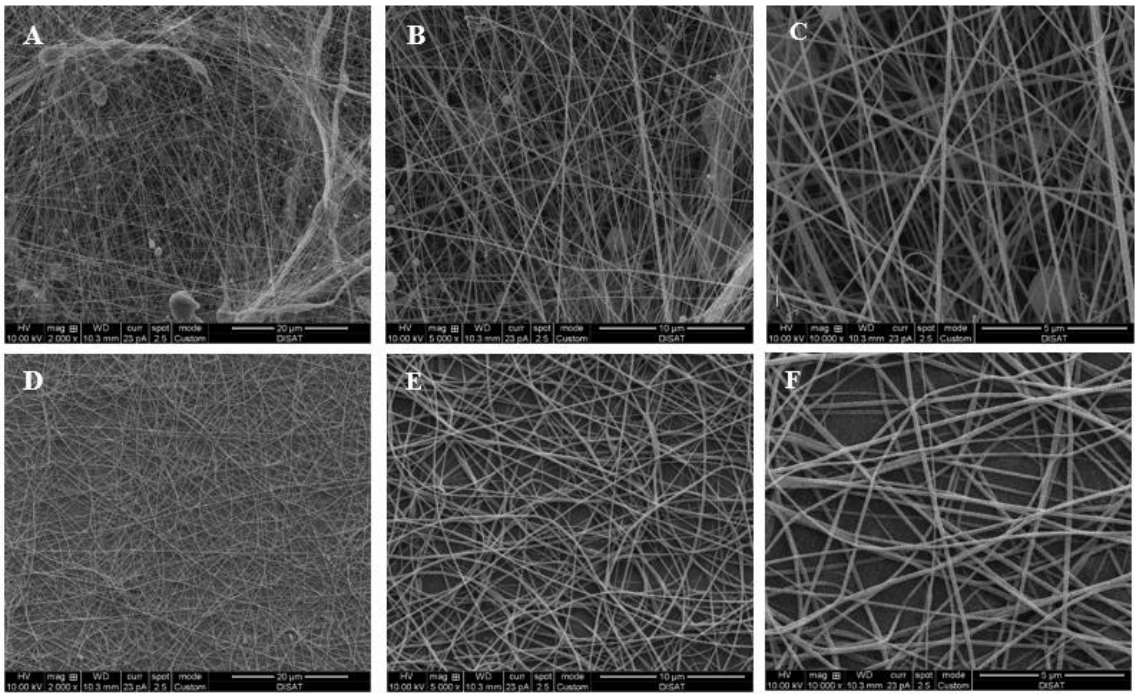

Figure 35. SEM images of electrospun membranes prepared following selected processing parameters: (A), (B), (C) Voltage: 15 kV, Distance: 12 cm and Flow rate: 0.25 mL/h at magnification 2000x (scale bar: 20 µm) , 5000x (scale bar: 10 µm) and 10000x (scale bar: 5 µm) respectively. (D), (E), (F) Voltage: 16 kV, Distance: 13 cm and Flow rate: 0.50 mL/h at magnification 2000x (scale bar: 20 µm) , 5000x (scale bar: 10 µm) and 10000x (scale bar: 5 µm) respectively.

Figure 35 shows the influence of slight variations of the process parameters on the fibers morphology. Images A, B and C show different magnifications of the membranes obtained setting an applied voltage of 15 kV, a distance needle-collector of 12 cm and a flow rate of 0.25 mL/h. Images show the presence of several beads of different sizes, ribbon-like structures and non-uniform morphology. Images D,E,F are related to membranes prepared at applied voltage of 16 kV, needle-collector distance (D) of 3 cm, flow rate of 0.5 mL/h. The obtained fibers were randomly distributed with uniform morphology and minimum presence of defects. Hence such processing parameters were selected for PCL scaffold fabrication.

3.2.2 ImageJ Software

Figure 36 B shows the percentage distribution of PCL fiber diameters: the diameters were comprised in a very narrow size range (40:240 nm) and most of the fibers (40%) had a diameter between 120 and 160 nm. All the analysed fibers had a diameter lower than 250 nm and the 37 % of the fibers showed a diameter lower than 120 nm. The average fiber diameter was 131±39 nm.

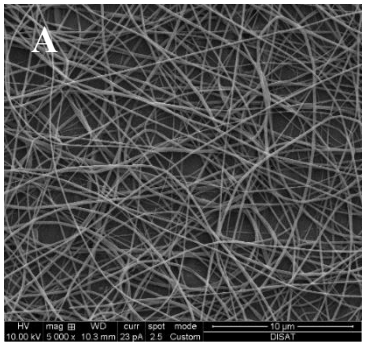

Average diameter	131 nm
Standard Deviation	39 nm

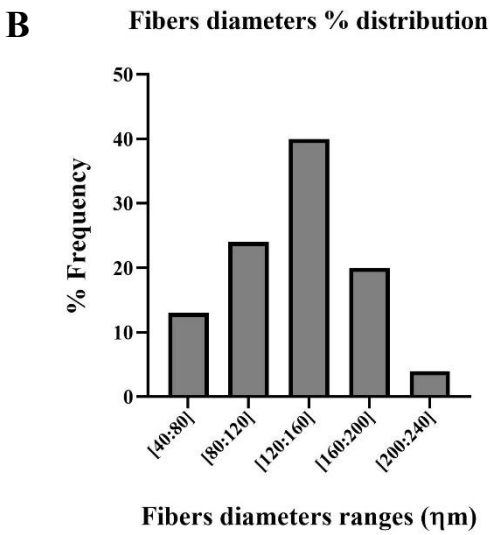

Figure 36. ImageJ data processing. (A) SEM image of membranes prepared from optimized set of parameters and average fiber diameter (131 ± 39 nm). (B) Percentage distribution of PCL fiber diameters.

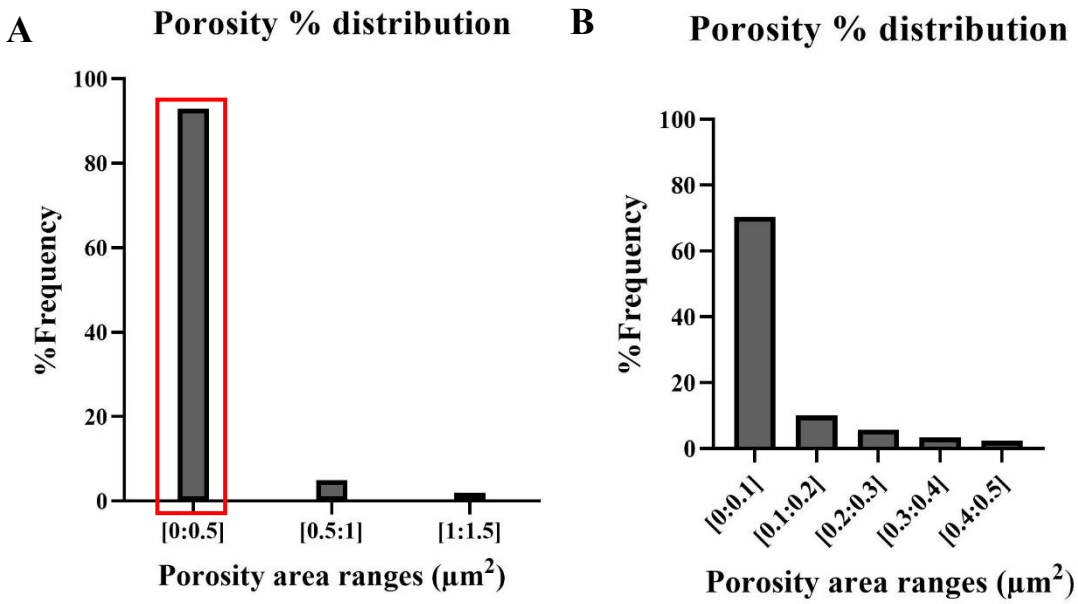

Figure 37. (A) Percentage distribution of electrospun PCL membrane porosities size. (B) Percentage distribution of electrospun PCL membrane porosities size in the range [0:0.5 µm2].

As shown in Figure 37, the obtained membranes had small and interconnected pores with small and homogeneously distributed sizes. About the 92% of pores area was in the range between 0 and 0.5 μm^2. Particularly, about 81% of pore area was less than 0.2 μm^2 . Fiber diameters and porosities distribution suggested high morphological uniformity of electrospun membranes implying that the scaffold could provide an uniform topographic stimulus to cells in culture.

3.3 Surface Modification Characterization

3.3.1 Immunofluorescence staining

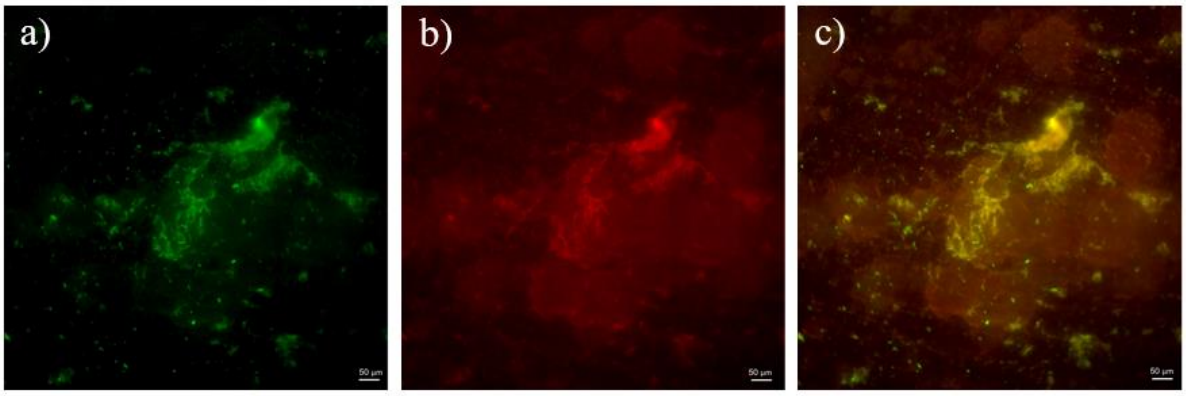

Figure 38. PCL-polyDOPA/C1F scaffold immunofluorescence staining: a) Fibronectin (labelled with AlexaFluor488), b) Collagen type I (labelled with AlexaFluor555), c) merged image. Bar scale 50

The images in Figure 38 show the morphology of the biomimetic protein coating and the spatial distribution of the two proteins on the scaffold surface. The protein spatial organization is due to the reciprocal fibrillogenesis of Collagen type I and Fibronectin, which leads to the packing of the two proteins [78].

3.3.2 BCA protein assay kit

BCA protein assay kit was performed in order to evaluate the effectiveness of the grafting of Collagen type I/Fibronectin on the adhesive polyDOPA pre-coating, previously deposited on the PCL-based scaffold. A calibration curve (Figure 39) was obtained relating the absorbance value of the standards (solutions at known protein concentration), obtained from the plate reader analysis, to their concentrations.

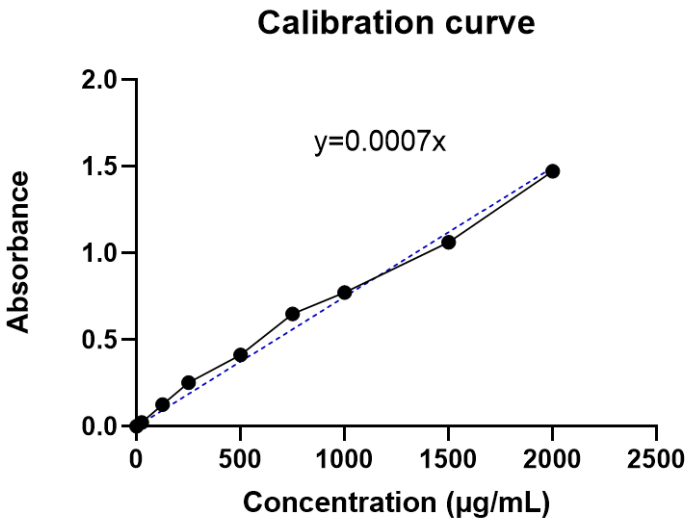

Figure 39. BCA protein assay kit calibration curve.

Using the calibration curve equation, the amount of coating proteins was calculated based on the absorbance values obtained by BCA assay (Figure 40).

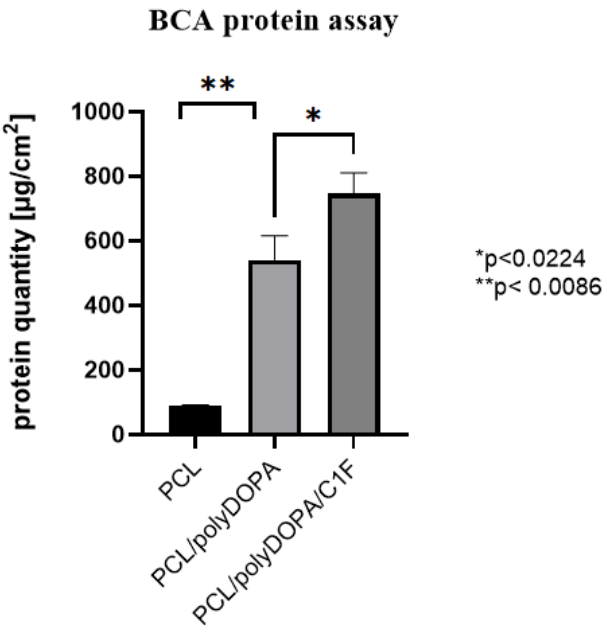

Figure 40. Protein quantity detected by BCA protein assay kit on NF-PCL, PCL/polyDOPA and PCL/PolyDOPA/C1F scaffolds.

The histogram in Figure 40 shows the effective deposition of the biomimetic coating based Collagen type I and Fibronectin (C1F) on the polyDOPA pre-adhesive coating, in terms of mass of proteins deposited for unit of exposed surface. Interestingly, protein quantity measured on PCL/polyDOPA/C1F samples (747 μg/cm^2) was higher than on PCL (88 μg/cm^2) and PCL/polyDOPA (541 μg/cm^2) samples, but included the contribution of polyDOPA layer and proteins of the biomimetic coating. Moreover, considering the initial quantity of proteins in the functionalizing solution (100 μg) and the average surface of each scaffold (1.13 cm^2), probably the contribution from residual Tris/HCl salts was also not negligible.

3.3.3 Coating stability test

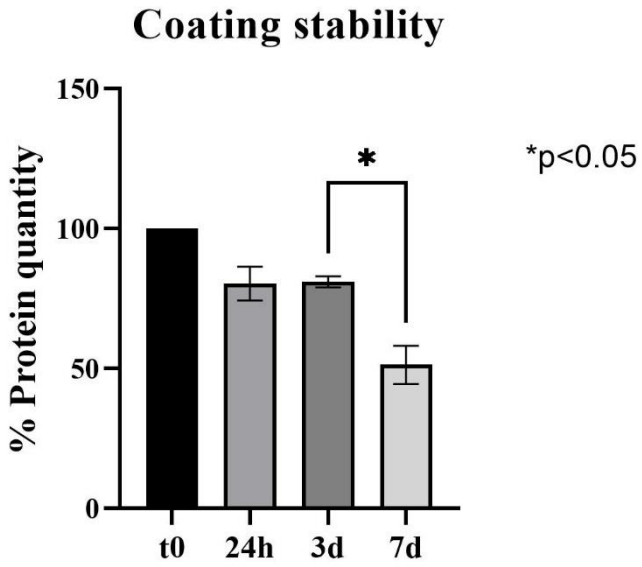

Figure 41. Protein quantity detected by BCA kit on the functionalized scaffold surface after incubation in physiological medium for different times: 24 h, 3 days and 7 days.

Figure 41 shows the percentage quantity of proteins detected on the scaffold surface after 1 d, 5 d and 7 d immersion in physiological medium. The percentages were calculated with respect to the initial quantity of proteins detected on the scaffold surface before the incubation period. This analysis was performed to evaluate the biomimetic coating stability during incubation in a physiological-like environment. In the first 24h immersion about the 20% of proteins detached from the surface, however subsequently the protein quantity on the scaffold surface remained constant up to 3 days. After 7 days immersion, about the 30% of proteins detached form the surface, this won't affect the eventual cell cultures as after 7 days cell would have already received adhesion and proliferation stimuli from the biomimetic coating and deposed their ECM. Thus, this results suggests coating stability in the first phases of cells adhesion.

3.4 Human cardiac fibroblasts culture on coated PCL substrates

3.4.1 Cytotoxicity assay

CytoTox-ONE™ Homogeneous Membrane Integrity Assay was used to evaluate *in vitro* the cytotoxicity of polyDOPA/Collagen type I/Fibronectin (PCL/polyDOPA/C1F) substrates. The assay was performed on the PCL/polyDOPA/C1F scaffold, on the naked PCL scaffolds and on coverslips coated with gelatin as control.

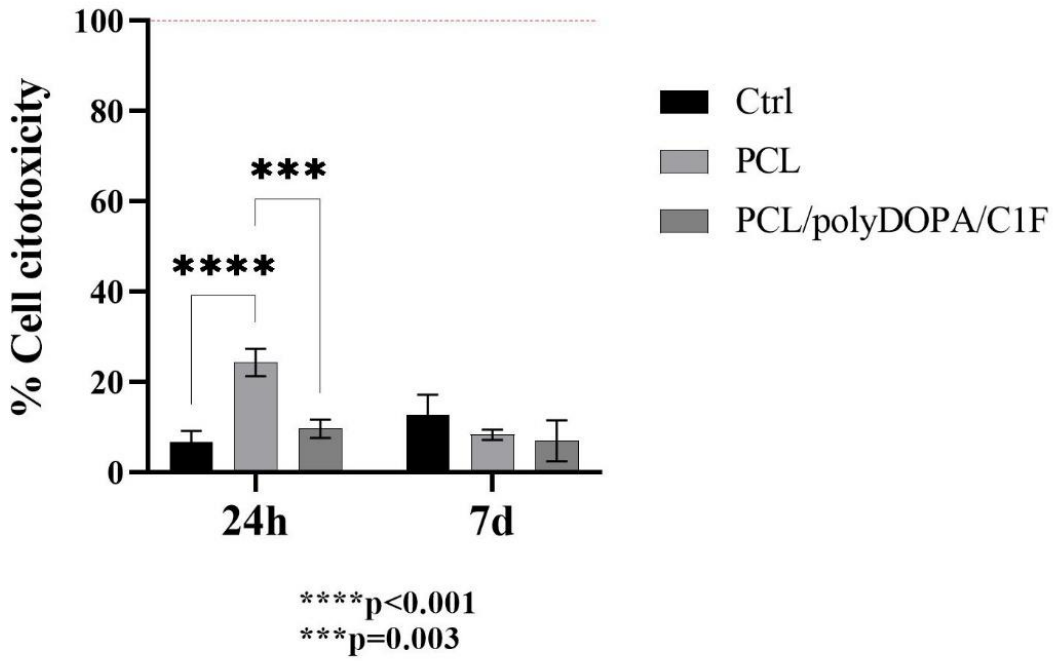

Figure 42.Cytotoxicity assay at 24 h, 3 d and 7 d of HCF culture on PCL fibers: non-functionalized (NF-PCL), functionalized with polyDOPA/Collagen type I/Fibronectin (PCL/polyDOPA/C1F) and on Gelatin-coated coverslips (CTRL). Percentages are referred to lysed samples.

Figure 42 shows the results of cytotoxicity assay performed after 24 h and 7 days culture of HCFs on non-functionalized PCL scaffolds, PCL/polyDOPA/C1F functionalized PCL scaffolds and on Gelatin coated coverslips. All the substrates were not cytotoxic for HCFs, suggesting their biocompatibility.

3.4.2 Cell Viability Assay

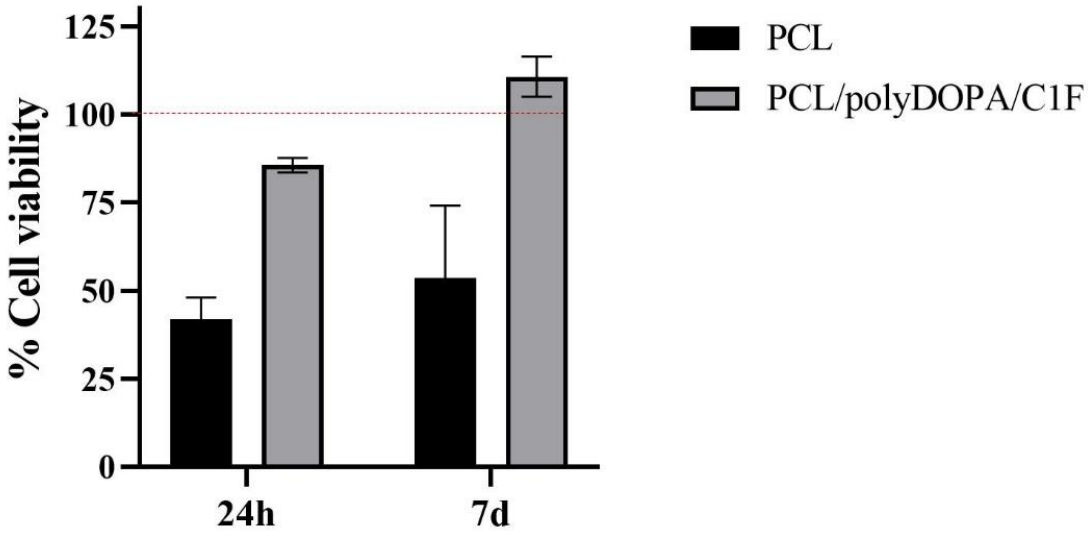

Figure 43. Cell viability assay of HCF at 24 h and 7 d culture 2D PCL fibers: non- functionalized (NF-PCL) and functionalized with polyDOPA/C1F (PCL/ polyDOPA/C1F). Percentages are referred to Gelatin-coated coverslips (CTRL).

Figure 43 shows cell viability after 24h and 7 days of culture on the 2D scaffolds: viability was higher for HCFs cultured on the substrates coated with the biomimetic coating (PCL/polyDOPA/C1F scaffolds), suggesting that the substrates biomimetic properties respect to the native pathological cardiac ECM allow to provide adhesion and proliferation stimuli to HFCs.

3.4.3 Phalloidin staining

Actin cytoskeletal organization and HCFs morphology were evaluated on PCL/polyDOPA/C1F scaffolds at 24 h and 7 days culture. Staining was performed in paraformaldehyde-fixed samples (NF-PCL and PCL-polyDOPA/C1F). Phalloidin staining of actin filaments showed that the surface properties of scaffolds were affected by the morphology and cytoskeletal organization of HCFs at different days of culture.

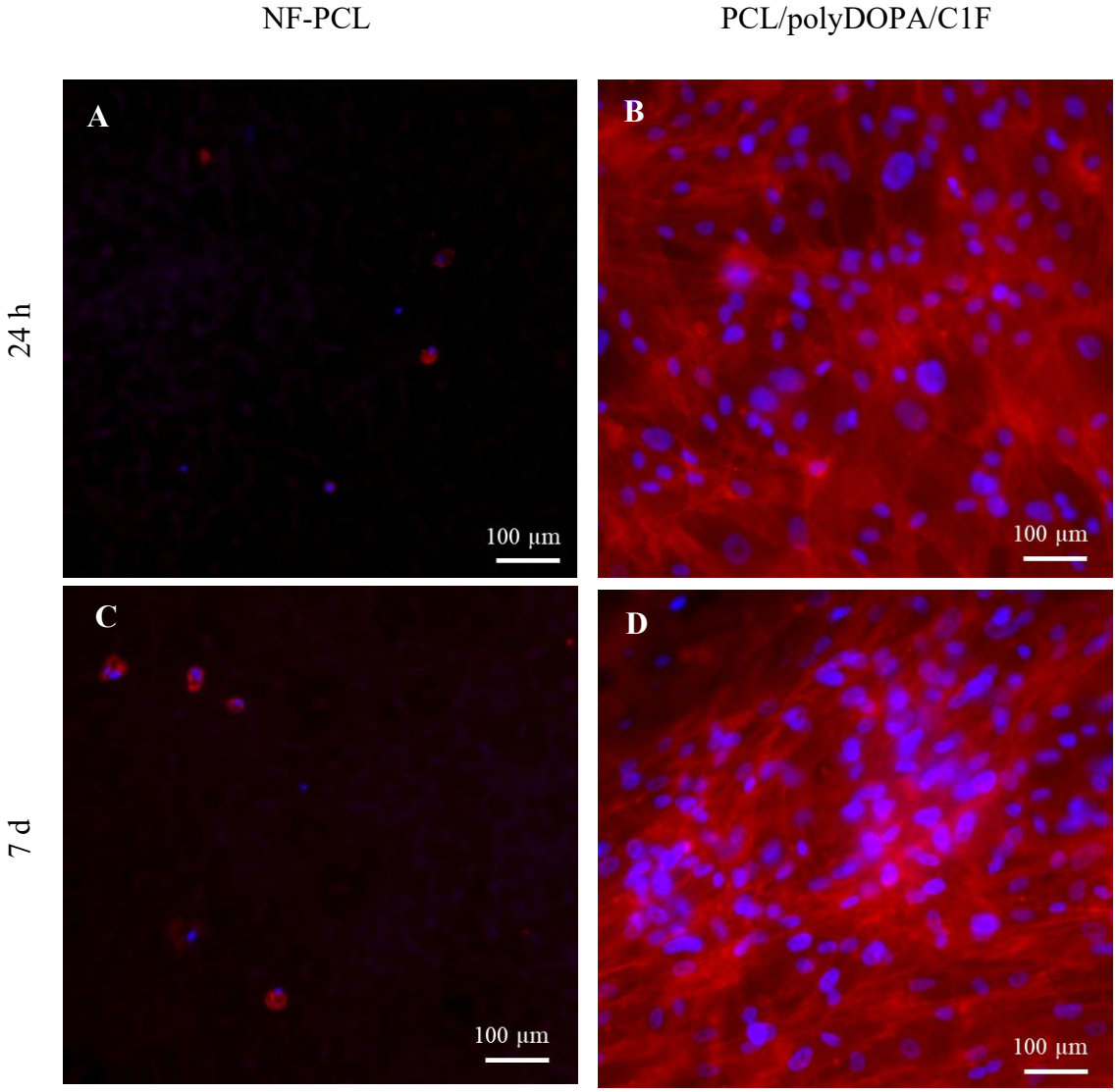

Figure 44..Merged Images: Phalloidin/DAPI staining for F-actin (red) and nuclei (blue) 7 days after seeding. (A-C) NF-PCL substrates, (B-D) PCL/polyDOPA/C1F.

Figure 44 shows the cytoskeletal actin filaments in red and the cell nuclei in blue. The cell nuclei were detectable after the treatment with DAPI dye, that is used to stain nuclei in fluorescence microscopy. DAPI is a fluorescent dye that binds selectively to double-stranded

DNA and forms strongly fluorescent DNA-DAPI complexes with high specificity. NF-PCL substrates did not promote cell attachment and proliferation (Figure 44 A,C). On the other hand, comparing Figure 44 B and C, related to PCL-polyDOPA/C1F scaffolds after 24 h and 7 days of culture respectively, it is possible to observe that after 7 days of culture cells appear to be have enhanced functional organization and morphology, since actin filaments are more stretched and oriented on the surface, suggesting that the PCL-polyDOPA/C1F scaffolds supported cell adhesion, spreading and time-dependent proliferation, after 7 days of culture.

4. Discussion

The fabrication of an *in vitro* model of cardiac fibrosis and its use in preclinical investigations is promising approach to study diseased myocardium after infarction and to test new therapies. The use of *in vitro* models could reduce the use of animal models, which are associated with ethical issues and show limited predictivity due to interspecies differences. The development of a suitable *in vitro* model of human cardiac fibrosis has been the focus of many studies, with the common goal to mimic the tissue specific architecture of the diseased myocardium. This thesis work was focused on the design and fabrication of a bidimensional *in vitro* model able to mimic cardiac tissue at early stages of cardiac fibrosis. Electrospinning technique was used to fabricate bioartificial PCL based scaffold with random morphology, to reproduce the architecture of the native cardiac extracellular matrix. The electrospinning protocol was optimized in terms of process parameters, in order to obtain nanofibrous scaffolds with a high percentage of fibers, uniform morphology, few defects and small pore size. The obtained electrospun nanofibrous membranes were characterized by random morphology, minimal presence of defects (Figure 35 D, E, F) small and uniformly distributed diameters (Figure 36 B) and small and interconnected porosities (Figure 37).

After broad literature research on pathological extracellular matrix composition, a biomimetic coating based on human Collagen type I (70%) and human Fibronectin (30%) was grafted on the electrospun scaffolds through a scaffold precoating obtained via a mussel-inspired strategy [23], [24]. In detail, self-polymerization of DOPA at pH 8.5 was exploited to pre-coat the scaffolds with polyDOPA, which exposes active catechol groups, useful for further functionalization reactions. PolyDOPA pre-coating of PCL membranes has been optimised in a previous thesis work [77]. The optimal time for Collagen type I/Fibronectin coating on PolyDOPA layer was established by QCM-D. In addition, QCM-D analyses allowed to demonstrate the successful Collagen type I/ Fibronectin grafting on the adhesive polyDOPA precoating (Figure 32) and to estimate the protein coating thickness, in prevision of the subsequent scaffold functionalization (Figure 33, Table 5).

Collagen type I/Fibronectin coating on PCL/PolyDOPA scaffolds was characterized by several analyses, such as immunofluoscence staining, colorimetric assay (BCA kit) and stability test in order to confirm and quantify protein deposition on scaffolds. Immunofluorescence showed the coating morphology and the spatial distribution of the two proteins, highlighting the reciprocal interaction between Collagen type I and Fibronectin, leading to reciprocal fibrillogenesis and

packing (Figure 38). Surface protein quantification, performed by BCA kit, allowed to confirm the effective deposition of the biomimetic coating on the adhesive polyDOPA pre-coating, showing an higher protein quantity on the PCL/polyDOPA/C1F samples with respect to PCL and PCL/polyDOPA samples (Figure 40). As regards coating stability evaluation, BCA kit analysis after 7 days incubation in physiological medium, showed a detachment from the surface of the scaffold of about 20% of proteins, compared to the initial protein amount, after 24 h. Nevertheless, it is interesting to highlight that subsequently the protein quantity on the scaffold surface remained constant up to 3 days and decreased of about 30% after 7 days incubation. This further decrease is negligible as after 7 days, cardiac fibroblast would have already deposited their ECM in response to the stimuli provided by the biomimetic coating. Thus, it is possible to deduce that the coating is stable in a physiological-like environment (Figure 41).

Finally, preliminary cellular tests were performed as biological validation of the proposed *in vitro* model. Cytotoxicity assay demonstrated that both non-functionalized PCL (NF-PCL) scaffolds and PCL-polyDOPA/C1F scaffolds are cytocompatible substrates, as, after 7 days culture of HCFs, they are characterized by a percent cytotoxicity of 9% and 7% respectively, with respect to a sample of lysed cells (maximum LDH release) (Figure 42). In addition, PCL-polyDOPA/C1F scaffolds seeded with HCFs were evaluated in terms of cell adhesion and proliferation. Since the initial step of seeding, 1 h after the deposition of the seeding volume on the surface of the scaffold, at the moment of culture medium addition, it is possible to observe that the biomimetic coating is effective in promoting early cell adhesion. Moreover, viability assay, performed after 24 h and 7 days culture of HCF, showed higher cell viability on PCL-polyDOPA/C1F substrates (87% after 24 h and 111% after 7 d, referring to the control) than on NF-PCL substrates (42% after 24 h and 54 % after 7d , referring to the control), suggesting first of all that the sterilization protocol didn't affect the coating integrity and that the PCL-polyDOPA/C1F scaffolds have high potential in stimulating cell adhesion proliferation (Figure 43). Phalloidin/DAPI staining was performed on PCL/polyDOPA/C1F and scaffolds at 24 h and 7 days of HCFs culture (Figure 44), in order to evaluate actin cytoskeletal organization and cells morphology. It emerged that NF-PCL scaffolds didn't support cells adhesion and proliferation while PCL/polyDOPA/C1F scaffolds were found to represent a suitable platform to support cell adhesion, spreading and time-dependent proliferation.

5. Conclusion and future developments

In conclusion, this study designed 2D biomimetic scaffolds to engineer *in vitro* bidimensional model of human cardiac fibrosis through scaffold cellularisation with human cardiac fibroblasts. Then model could help to better understand tissue pathophysiology and to obtain a powerful platform for disease screening and preclinical therapy testing. As further progress in this research, it could be interesting to graft the biomimetic protein coating, based on Collagen type I and Fibronectin, on aligned electrospun PCL nanofibers, in order to mimic the late stages of cardiac fibrosis and to monitor disease advances. A study of the effect of topographic stimuli on cell organization and protein expression should be carried out as it would be interesting to conduct long-term cell culture both on the functionalized random and aligned nanofibers, monitoring fibrotic markers expression. In addition, a bioreactor could be used to culture the cells under dynamic culture condition to reproduce the complexity of the native microenvironment. Finally, this model could be used as platform to test direct reprogramming therapy based on miRNA, in order to induce a phenotypical switch from cardiac fibroblasts to cardiomyocytes, with the goal to regenerate the infarcted myocardium after MI into functional beating tissue.

References

[1] M. Sharma and J. R. Teerlink, "A rational approach for the treatment of acute heart failure: Current strategies and future options," *Curr. Opin. Cardiol.*, vol. 19, no. 3, pp. 254–263, 2004, doi: 10.1097/00001573-200405000-00011.

[2] W. W. Chen *et al.*, "China cardiovascular diseases report 2015: A summary," *J. Geriatr. Cardiol.*, vol. 14, no. 1, pp. 1–10, 2017, doi: 10.11909/j.issn.1671-5411.2017.01.012.

[3] P. Rossignol, A. F. Hernandez, S. D. Solomon, and F. Zannad, "Heart failure drug treatment," *Lancet*, vol. 393, no. 10175, pp. 1034–1044, 2019, doi: 10.1016/S0140-6736(18)31808-7.

[4] W. Lesyuk, C. Kriza, and P. Kolominsky-Rabas, "Cost-of-illness studies in heart failure: A systematic review 2004-2016," *BMC Cardiovasc. Disord.*, vol. 18, no. 1, pp. 1–11, 2018, doi: 10.1186/s12872-018-0815-3.

[5] S. S. Virani *et al.*, *Heart disease and stroke statistics—2020 update: A report from the American Heart Association*. 2020.

[6] Q. Z. Chen, S. E. Harding, N. N. Ali, A. R. Lyon, and A. R. Boccaccini, "Biomaterials in cardiac tissue engineering: Ten years of research survey," *Mater. Sci. Eng. R Reports*, vol. 59, no. 1–6, pp. 1–37, 2008, doi: 10.1016/j.mser.2007.08.001.

[7] S. Park, N. B. Nguyen, A. Pezhouman, and R. Ardehali, "Cardiac fibrosis: potential therapeutic targets," *Transl. Res.*, vol. 209, pp. 121–137, 2019, doi: 10.1016/j.trsl.2019.03.001.

[8] P. Ponikowski *et al.*, "2016 ESC Guidelines for the diagnosis and treatment of acute and chronic heart failure," *Eur. Heart J.*, vol. 37, no. 27, pp. 2129-2200m, 2016, doi: 10.1093/eurheartj/ehw128.

[9] F. A. van Nieuwenhoven and N. A. Turner, "The role of cardiac fibroblasts in the transition from inflammation to fibrosis following myocardial infarction," *Vascul. Pharmacol.*, vol. 58, no. 3, pp. 182–188, 2013, doi: 10.1016/j.vph.2012.07.003.

[10] N. G. Frangogiannis, "The inflammatory response in myocardial injury, repair, and remodelling," *Nat. Rev. Cardiol.*, vol. 11, no. 5, pp. 255–265, 2014, doi: 10.1038/nrcardio.2014.28.

[11] M. G. St. John Sutton and N. Sharpe, "Left ventricular remodeling after myocardial infarction: Pathophysiology and therapy," *Circulation*, vol. 101, no. 25, pp. 2981–2988, 2000, doi: 10.1161/01.cir.101.25.2981.

[12] S. W. M. Van Den Borne, J. Diez, W. M. Blankesteijn, J. Verjans, L. Hofstra, and J. Narula,

"Myocardial remodeling after infarction: The role of myofibroblasts," *Nat. Rev. Cardiol.*, vol. 7, no. 1, pp. 30–37, 2010, doi: 10.1038/nrcardio.2009.199.

[13] P. Zhou and W. T. Pu, "Recounting cardiac cellular composition," *Circ. Res.*, vol. 118, no. 3, pp. 368–370, 2016, doi: 10.1161/CIRCRESAHA.116.308139.

[14] E. A. Woodcock and S. J. Matkovich, "Cardiomyocytes structure, function and associated pathologies," *Int. J. Biochem. Cell Biol.*, vol. 37, no. 9, pp. 1746–1751, 2005, doi: 10.1016/j.biocel.2005.04.011.

[15] T. A. Baudino, W. Carver, W. Giles, and T. K. Borg, "Cardiac fibroblasts: Friend or foe?," *Am. J. Physiol. - Hear. Circ. Physiol.*, vol. 291, no. 3, 2006, doi: 10.1152/ajpheart.00023.2006.

[16] C. A. Souders, S. L. K. Bowers, and T. A. Baudino, "Cardiac fibroblast: The renaissance cell," *Circ. Res.*, vol. 105, no. 12, pp. 1164–1176, 2009, doi: 10.1161/CIRCRESAHA.109.209809.

[17] M. Hegarová, I. Málek, and J. Kautzner, "Changes in the extracellular matrix during myocardial remodelling," *Exp. Clin. Cardiol.*, vol. 20, no. 1, pp. 771–778, 2014, doi: 10.4172/2368-0512.1000026.

[18] K. E. Porter and N. A. Turner, "Cardiac fibroblasts: At the heart of myocardial remodeling," *Pharmacol. Ther.*, vol. 123, no. 2, pp. 255–278, 2009, doi: 10.1016/j.pharmthera.2009.05.002.

[19] D. Fan, A. Takawale, J. Lee, and Z. Kassiri, "Cardiac fibroblasts, fibrosis and extracellular matrix remodeling in heart disease," *Fibrogenes. Tissue Repair*, vol. 5, no. 1, pp. 1–13, 2012, doi: 10.1186/1755-1536-5-15.

[20] N. G. Frangogiannis, "The extracellular matrix in ischemic and nonischemic heart failure," *Circ. Res.*, vol. 125, no. 1, pp. 117–146, 2019, doi: 10.1161/CIRCRESAHA.119.311148.

[21] J. P. M. Cleutjens and E. E. J. M. Creemers, "Integration of concepts: Cardiac extracellular matrix remodeling after myocardial infarction," *J. Card. Fail.*, vol. 8, no. 6 SUPPL., pp. 344–348, 2002, doi: 10.1054/jcaf.2002.129261.

[22] A. Takawale, S. S. V. P. Sakamuri, and Z. Kassiri, "Extracellular matrix communication and turnover in cardiac physiology and pathology," *Compr. Physiol.*, vol. 5, no. 2, pp. 687–719, 2015, doi: 10.1002/cphy.c140045.

[23] D. Bejleri and M. E. Davis, "Decellularized Extracellular Matrix Materials for Cardiac Repair and Regeneration," *Adv. Healthc. Mater.*, vol. 8, no. 5, pp. 1–29, 2019, doi: 10.1002/adhm.201801217.

[24] R. I. Bashey, A. Martinez-Hernandez, and S. A. Jimenez, "Isolation, characterization, and localization of cardiac collagen type VI: Associations with other extracellular matrix

components," *Circ. Res.*, vol. 70, no. 5, pp. 1006–1017, 1992, doi: 10.1161/01.res.70.5.1006.

[25] M. Nguyen-Truong and Z. Wang, "Biomechanical properties and mechanobiology of cardiac ECM," *Adv. Exp. Med. Biol.*, vol. 1098, pp. 1–19, 2018, doi: 10.1007/978-3-319-97421-7_1.

[26] S. L. K. Bowers, I. Banerjee, and T. A. Baudino, "The extracellular matrix: At the center of it all," *J. Mol. Cell. Cardiol.*, vol. 48, no. 3, pp. 474–482, 2010, doi: 10.1016/j.yjmcc.2009.08.024.

[27] A. H. Sadeghi *et al.*, "Engineered 3D Cardiac Fibrotic Tissue to Study Fibrotic Remodeling," *Adv. Healthc. Mater.*, vol. 6, no. 11, pp. 1–14, 2017, doi: 10.1002/adhm.201601434.

[28] V. Talman and H. Ruskoaho, "Cardiac fibrosis in myocardial infarction—from repair and remodeling to regeneration," *Cell Tissue Res.*, vol. 365, no. 3, pp. 563–581, 2016, doi: 10.1007/s00441-016-2431-9.

[29] P. Kong, P. Christia, and N. G. Frangogiannis, "The pathogenesis of cardiac fibrosis," *Cell. Mol. Life Sci.*, vol. 71, no. 4, pp. 549–574, 2014, doi: 10.1007/s00018-013-1349-6.

[30] J. J. Tomasek, G. Gabbiani, B. Hinz, C. Chaponnier, and R. A. Brown, "Myofibroblasts and mechano: Regulation of connective tissue remodelling," *Nat. Rev. Mol. Cell Biol.*, vol. 3, no. 5, pp. 349–363, 2002, doi: 10.1038/nrm809.

[31] J. Leor, Y. Amsalem, and S. Cohen, "Cells, scaffolds, and molecules for myocardial tissue engineering," *Pharmacol. Ther.*, vol. 105, no. 2, pp. 151–163, 2005, doi: 10.1016/j.pharmthera.2004.10.003.

[32] T. E. Robey, M. K. Saiget, H. Reinecke, and C. E. Murry, "Systems approaches to preventing transplanted cell death in cardiac repair," *J. Mol. Cell. Cardiol.*, vol. 45, no. 4, pp. 567–581, 2008, doi: 10.1016/j.yjmcc.2008.03.009.

[33] R. Chaudhuri, M. Ramachandran, P. Moharil, M. Harumalani, and A. K. Jaiswal, "Biomaterials and cells for cardiac tissue engineering: Current choices," *Mater. Sci. Eng. C*, vol. 79, pp. 950–957, 2017, doi: 10.1016/j.msec.2017.05.121.

[34] J. V. Robert P. Lanza, Robert Langer, *Principles of Tissue Engineering*, Second Edi. Academic Press.

[35] L. G. Griffith and G. Naughton, "Tissue engineering - Current challenges and expanding opportunities," *Science (80-.).*, vol. 295, no. 5557, 2002, doi: 10.1126/science.1069210.

[36] R. L. Carrier *et al.*, "Cardiac tissue engineering: Cell seeding, cultivation parameters, and tissue construct characterization," *Biotechnol. Bioeng.*, vol. 64, no. 5, pp. 580–589, 1999, doi: 10.1002/(SICI)1097-0290(19990905)64:5<580::AID-BIT8>3.0.CO;2-X.

[37] K. H. Benam *et al.*, “Engineered in vitro disease models,” *Annu. Rev. Pathol. Mech. Dis.*, vol. 10, pp. 195–262, 2015, doi: 10.1146/annurev-pathol-012414-040418.

[38] G. Vunjak Novakovic, T. Eschenhagen, and C. Mummery, “Myocardial tissue engineering: In vitro models,” *Cold Spring Harb. Perspect. Med.*, vol. 4, no. 3, pp. 1–16, 2014, doi: 10.1101/cshperspect.a014076.

[39] J. C. Deddens *et al.*, “Modeling the Human Scarred Heart In Vitro: Toward New Tissue Engineered Models,” *Adv. Healthc. Mater.*, vol. 6, no. 3, pp. 1–21, 2017, doi: 10.1002/adhm.201600571.

[40] T. C. L. Bracco Gartner *et al.*, “Anti-fibrotic Effects of Cardiac Progenitor Cells in a 3D-Model of Human Cardiac Fibrosis,” *Front. Cardiovasc. Med.*, vol. 6, 2019, doi: 10.3389/fcvm.2019.00052.

[41] H. Kristin M. French, Archan V. Boopathy, Jessica A. DeQuach, Loice Chingozha and and M. E. D. Luc, Karen L. Christman, “A Naturally-Derived Cardiac Extracellular Matrix Enhances Cardiac Progenitor Cell Behavior In Vitro,” *Acta Biomateralia*, vol. 8, no. 12, pp. 4357–4364, 2012, doi: doi:10.1016/j.actbio.2012.07.033.

[42] R. M. Wang and K. L. Christman, “Decellularized myocardial matrix hydrogels: In basic research and preclinical studies,” *Adv. Drug Deliv. Rev.*, vol. 96, pp. 77–82, 2016, doi: 10.1016/j.addr.2015.06.002.

[43] J. Hjortnaes *et al.*, “Directing valvular interstitial cell myofibroblast-like differentiation in a hybrid hydrogel platform,” *Adv. Healthc. Mater.*, vol. 4, no. 1, pp. 121–130, 2015, doi: 10.1002/adhm.201400029.

[44] H. Saini, A. Navaei, A. Van Putten, and M. Nikkhah, “3D Cardiac Microtissues Encapsulated with the Co-Culture of Cardiomyocytes and Cardiac Fibroblasts,” *Adv. Healthc. Mater.*, vol. 4, no. 13, pp. 1961–1971, 2015, doi: 10.1002/adhm.201500331.

[45] F. Poobalarahi, C. F. Baicu, and A. D. Bradshaw, “Cardiac myofibroblasts differentiated in 3D culture exhibit distinct changes in collagen I production, processing, and matrix deposition,” *Am. J. Physiol. - Hear. Circ. Physiol.*, vol. 291, no. 6, pp. 2924–2933, 2006, doi: 10.1152/ajpheart.00153.2006.

[46] P. Dell’Era, “Cardiac disease modeling using induced pluripotent stem cell-derived human cardiomyocytes,” *World J. Stem Cells*, vol. 7, no. 2, p. 329, 2015, doi: 10.4252/wjsc.v7.i2.329.

[47] A. Mathur, Z. Ma, P. Loskill, S. Jeeawoody, and K. E. Healy, “In vitro cardiac tissue models: Current status and future prospects,” *Adv. Drug Deliv. Rev.*, vol. 96, pp. 203–213, 2016, doi: 10.1016/j.addr.2015.09.011.

[48] P. W. Burridge, G. Keller, J. D. Gold, and J. C. Wu, "Production of de novo cardiomyocytes: Human pluripotent stem cell differentiation and direct reprogramming," *Cell Stem Cell*, vol. 10, no. 1, pp. 16–28, 2012, doi: 10.1016/j.stem.2011.12.013.

[49] M. O. Lee *et al.*, "Modelling cardiac fibrosis using three-dimensional cardiac microtissues derived from human embryonic stem cells," *J. Biol. Eng.*, vol. 13, no. 1, pp. 1–17, 2019, doi: 10.1186/s13036-019-0139-6.

[50] H. Zhang *et al.*, "Generation of quiescent cardiac fibroblasts from human induced pluripotent stem cells for in vitro modeling of cardiac fibrosis," *Circ. Res.*, vol. 125, no. 5, pp. 552–566, 2019, doi: 10.1161/CIRCRESAHA.119.315491.

[51] Y. S. Zhang *et al.*, "From cardiac tissue engineering to heart-on-a-chip: Beating challenges," *Biomed. Mater.*, vol. 10, no. 3, p. 34006, 2015, doi: 10.1088/1748-6041/10/3/034006.

[52] M. Kong *et al.*, "Cardiac Fibrotic Remodeling on a Chip with Dynamic Mechanical Stimulation," *Adv. Healthc. Mater.*, vol. 8, no. 3, pp. 1–13, 2019, doi: 10.1002/adhm.201801146.

[53] P. Occhetta *et al.*, "A three-dimensional: In vitro dynamic micro-tissue model of cardiac scar formation," *Integr. Biol. (United Kingdom)*, vol. 10, no. 3, pp. 174–183, 2018, doi: 10.1039/c7ib00199a.

[54] A. H. Sadeghi *et al.*, "Engineered Three-Dimensional Cardiac Fibrotic Tissue to Study Fibrotic Remodeling," *Adv. Healthc. Mater.*, vol. 6, no. 11, pp. 11–39, 2017, doi: 10.1002/adhm.201601434.Engineered.

[55] A. Gandaglia *et al.*, "Cardiomyocytes in vitro adhesion is actively influenced by biomimetic synthetic peptides for cardiac tissue engineering," *Tissue Eng. - Part A*, vol. 18, no. 7–8, pp. 725–736, 2012, doi: 10.1089/ten.tea.2011.0254.

[56] N. R. Richbourg, N. A. Peppas, and V. I. Sikavitsas, "Tuning the biomimetic behavior of scaffolds for regenerative medicine through surface modifications," *J. Tissue Eng. Regen. Med.*, vol. 13, no. 8, pp. 1275–1293, 2019, doi: 10.1002/term.2859.

[57] S. Hinderer, S. L. Layland, and K. Schenke-Layland, "ECM and ECM-like materials - Biomaterials for applications in regenerative medicine and cancer therapy," *Adv. Drug Deliv. Rev.*, vol. 97, pp. 260–269, 2016, doi: 10.1016/j.addr.2015.11.019.

[58] S. M. LaNasa and S. J. Bryant, "Influence of ECM proteins and their analogs on cells cultured on 2-D hydrogels for cardiac muscle tissue engineering," *Acta Biomater.*, vol. 5, no. 8, pp. 2929–2938, 2009, doi: 10.1016/j.actbio.2009.05.011.

[59] C. Alperin, P. W. Zandstra, and K. A. Woodhouse, "Polyurethane films seeded with embryonic

stem cell-derived cardiomyocytes for use in cardiac tissue engineering applications," *Biomaterials*, vol. 26, no. 35, pp. 7377–7386, 2005, doi: 10.1016/j.biomaterials.2005.05.064.

[60] A. Moorthi, Y. C. Tyan, and T. W. Chung, "Surface-modified polymers for cardiac tissue engineering," *Biomater. Sci.*, vol. 5, no. 10, pp. 1976–1987, 2017, doi: 10.1039/c7bm00309a.

[61] M. L. Decaris, B. Y. Binder, M. A. Soicher, A. Bhat, and J. K. Leach, "Cell-derived matrix coatings for polymeric scaffolds," *Tissue Eng. - Part A*, vol. 18, no. 19–20, pp. 2148–2157, 2012, doi: 10.1089/ten.tea.2011.0677.

[62] A. Arnau, "A review of interface electronic systems for AT-cut quartz crystal microbalance applications in liquids," *Sensors*, vol. 8, no. 1, pp. 370–411, 2008, doi: 10.3390/s8010370.

[63] S. Bruckenstein and M. Shay, "Experimental aspects of use of the quartz crystal microbalance in solution," *Electrochim. Acta*, vol. 30, no. 10, pp. 1295–1300, 1985, doi: 10.1016/0013-4686(85)85005-2.

[64] M. C. Dixon, "Quartz crystal microbalance with dissipation monitoring: Enabling real-time characterization of biological materials and their interactions," *J. Biomol. Tech.*, vol. 19, no. 3, pp. 151–158, 2008.

[65] T. M. Jayawardena *et al.*, "MicroRNA induced cardiac reprogramming in vivo evidence for mature cardiac myocytes and improved cardiac function," *Circ. Res.*, vol. 116, no. 3, pp. 418–424, 2014, doi: 10.1161/CIRCRESAHA.116.304510.

[66] N. Muraoka and M. Ieda, "Direct reprogramming of fibroblasts into myocytes to reverse fibrosis," *Annu. Rev. Physiol.*, vol. 76, no. September 2013, pp. 21–37, 2014, doi: 10.1146/annurev-physiol-021113-170301.

[67] Y. P. Kong, B. Carrion, R. K. Singh, and A. J. Putnam, "Matrix identity and tractional forces influence indirect cardiac reprogramming," *Sci. Rep.*, vol. 3, pp. 1–13, 2013, doi: 10.1038/srep03474.

[68] S. M. S. Shahriar, J. Mondal, M. N. Hasan, V. Revuri, D. Y. Lee, and Y. K. Lee, "Electrospinning nanofibers for therapeutics delivery," *Nanomaterials*, vol. 9, no. 4, 2019, doi: 10.3390/nano9040532.

[69] A. Valizadeh and S. M. Farkhani, "Electrospinning and electrospun nanofibres," *IET Nanobiotechnology*, vol. 8, no. 2, pp. 83–92, 2014, doi: 10.1049/iet-nbt.2012.0040.

[70] N. Bhardwaj and S. C. Kundu, "Electrospinning: A fascinating fiber fabrication technique," *Biotechnol. Adv.*, vol. 28, no. 3, pp. 325–347, 2010, doi: 10.1016/j.biotechadv.2010.01.004.

[71] D. Li and Y. Xia, "Electrospinning of nanofibers: Reinventing the wheel?," *Adv. Mater.*, vol. 16,

no. 14, pp. 1151–1170, 2004, doi: 10.1002/adma.200400719.

[72] T. Subbiah, G. S. Bhat, R. W. Tock, S. Parameswaran, and S. S. Ramkumar, “Electrospinning of nanofibers,” *J. Appl. Polym. Sci.*, vol. 96, no. 2, pp. 557–569, 2005, doi: 10.1002/app.21481.

[73] M. Shin, O. Ishii, T. Sueda, and J. P. Vacanti, “Contractile cardiac grafts using a novel nanofibrous mesh,” *Biomaterials*, vol. 25, no. 17, pp. 3717–3723, 2004, doi: 10.1016/j.biomaterials.2003.10.055.

[74] G. Zhao, X. Zhang, T. J. Lu, and F. Xu, “Recent Advances in Electrospun Nanofibrous Scaffolds for Cardiac Tissue Engineering,” *Adv. Funct. Mater.*, vol. 25, no. 36, pp. 5726–5738, 2015, doi: 10.1002/adfm.201502142.

[75] M. Kitsara, O. Agbulut, D. Kontziampasis, Y. Chen, and P. Menasché, “Fibers for hearts: A critical review on electrospinning for cardiac tissue engineering,” *Acta Biomater.*, vol. 48, pp. 20–40, 2017, doi: 10.1016/j.actbio.2016.11.014.

[76] D. Kai, M. P. Prabhakaran, G. Jin, and S. Ramakrishna, “Guided orientation of cardiomyocytes on electrospun aligned nanofibers for cardiac tissue engineering,” *J. Biomed. Mater. Res. - Part B Appl. Biomater.*, vol. 98 B, no. 2, pp. 379–386, 2011, doi: 10.1002/jbm.b.31862.

[77] I. Carmagnola *et al.*, “Plga membranes functionalized with gelatin through biomimetic mussel-inspired strategy,” *Nanomaterials*, vol. 10, no. 11, pp. 1–17, 2020, doi: 10.3390/nano10112184.

[78] J. A. Paten *et al.*, “Molecular Interactions between Collagen and Fibronectin: A Reciprocal Relationship that Regulates De Novo Fibrillogenesis,” *Chem*, vol. 5, no. 8, pp. 2126–2145, 2019, doi: 10.1016/j.chempr.2019.05.011.

Ringraziamenti

Sono arrivata alla fine di questo straordinario percorso, che sembrava lunghissimo e disseminato di infiniti ostacoli. È davvero importante per me esprimere la gratitudine verso tutte le persone che mi hanno aiutato a superare ogni difficoltà e che mi hanno permesso di raggiungere questo traguardo.

Voglio ringraziare la Professoressa Chiono per avermi dato l'opportunità di partecipare a un progetto così importante e stimolante come BIORECAR, che mi ha dato l'occasione di imparare, crescere e di continuare ad innamorarmi della ricerca. Ringrazio l'Ingegnere Gerardina Ruocco, che mi ha seguito passo dopo passo, sempre al mio fianco, pronta a rassicurarmi e a indirizzami, sempre paziente e disponibile. Ringrazio la Dottoressa Irene Carmagnola per il supporto e la disponibilità e la Dottoressa Zoso per avermi introdotto con passione e pazienza al mondo della Biologia. Ringrazio Francesca, che in questi interminabili mesi ha condiviso le mie ansie, sempre pronta a tranquillizzarmi e a capirmi.

La mia più profonda gratitudine va alla mia famiglia, che mi ha sempre permesso di inseguire i miei sogni, che ha sempre creduto in me e che giorno dopo giorno mi ha accompagnato in questo percorso, anche da lontano. Il vostro continuo supporto e la vostra fiducia incondizionata mi hanno permesso di superare ostacoli che sembravano insormontabili. Non potrò mai ringraziarvi abbastanza per avermi sempre messo al primo posto, per avermi dato il mondo senza mai chiedere nulla in cambio e per avermi fatto diventare la persona che sono.

Ringrazio la meravigliosa famiglia di Via Morghen 21, che ha reso indimenticabile questi anni, mi avete fatto sentire meno lontana da casa. Le nostre cene e i weekend passati a cucinare l'impossibile hanno rappresentato per me la migliore valvola di sfogo che potesse esistere, ogni preoccupazione spariva. In particolare voglio ringraziare Bartolomeo, per i suoi saggi consigli, per essere sempre stato un punto di riferimento e per avermi sempre aiutato a superare e razionalizzare i mille problemi che mi si presentavano, Francesco, per tutte le pause caffè e per aver sempre creduto in me, Alice, per essere stata la mia coinquilina del cuore, per gli abbracci sotto il piumone e per la sua infinita dolcezza. Voglio ringraziare la mia migliore amica, Eleonora, che è entrata a far parte di questa bellissima famiglia e nell'ultimo anno è stata sempre al mio fianco, sempre pronta a incoraggiarmi, a sopportarmi e a detonare le mie crisi di panico.

Ringrazio il fantastico gruppo Cinquantena, Bartolomeo, Eleonora, Gabriele e Vera, in un periodo difficile e buio come il lockdown siete riusciti a farmi vivere uno dei periodi più veri della mia vita.

Ringrazio le mie compagne di avventura, Carla e Erika. Da quando vi ho incontrato è diventato tutto più luminoso, mi avete insegnato che non bisogna conoscersi da una vita per costruire un'amicizia vera. Grazie per aver sempre creduto in me, per avermi incoraggiato e per aver sopportato le mie infinite paure e paranoie.

Ringrazio les italiens a Besançon del mio cuore: Chiara, Giada, Eigi, Safaa, Giovanni, Giuseppe ed Ermando, siete stati la luce del mio Erasmus, grazie di avermi aiutata a sopravvivere alla Francia Merda, non ce l'avrei fatta senza di voi.

In fine, ma non per importanza vorrei ringraziare Parvati, l'ultima arrivata in Via Morghen, che in questi pochi mesi è stata la mia compagna di uscite, grazie per avermi regalato tanta spensieratezza nel periodo in cui ne avevo più bisogno.

Grazie Torino, sei e sarai per sempre la mia seconda casa.